



Impact of soil water content on the overturning resistance of young *Pinus Pinaster* in sandy soil

Pauline Défossez, G. Veylon, M. Yang, Jean-Marc Bonnefond, Didier Garrigou, P. Trichet, Frédéric Danjon

► To cite this version:

Pauline Défossez, G. Veylon, M. Yang, Jean-Marc Bonnefond, Didier Garrigou, et al.. Impact of soil water content on the overturning resistance of young *Pinus Pinaster* in sandy soil. *Forest Ecology and Management*, 2021, 480, pp.1-13. 10.1016/j.foreco.2020.118614 . hal-03106706

HAL Id: hal-03106706

<https://hal.inrae.fr/hal-03106706>

Submitted on 17 Oct 2022

HAL is a multi-disciplinary open access archive for the deposit and dissemination of scientific research documents, whether they are published or not. The documents may come from teaching and research institutions in France or abroad, or from public or private research centers.

L'archive ouverte pluridisciplinaire **HAL**, est destinée au dépôt et à la diffusion de documents scientifiques de niveau recherche, publiés ou non, émanant des établissements d'enseignement et de recherche français ou étrangers, des laboratoires publics ou privés.



Distributed under a Creative Commons Attribution - NonCommercial 4.0 International License

Impact of soil water content on the overturning resistance of young *Pinus Pinaster* in sandy soil

P. Défossez^{a,*}, G. Veylon^b, M. Yang^a, J.M. Bonnefond^a, D. Garrigou^a,
P. Trichet^a, F. Danjon^c

^aINRAE, Bordeaux Sciences Agro, ISPA, F-33882, Villenave d'Ornon, France

^bINRAE, Aix Marseille Univ., RECOVER, F-13182, Aix-en-Provence, France

^cINRAE, Univ. Bordeaux, BIOGECO, F-33610, Cestas, France

Abstract

Background and aims. The tree resistance to uprooting is crucial to face wind damage in temperate forest. Tree anchorage varies considerably with site conditions, species, and tree age. Only few studies have focused on the influence of the site soil properties on the tree anchorage. With ongoing climate change, the soil hydrologic conditions are changing in Europe due to higher precipitations during winter, with possible higher risk of wind damage in forests.

Methods. This study investigates the role of soil hydrology on tree anchorage of *Pinus pinaster* in sandy soil with a combination of field experiments and simulations. Tree pulling experiments until root-soil system failure were performed for 12 *Pinus pinaster* of 14 years-old growing in podzol to measure the tree resistance to uprooting M_c for two contrasted soil water conditions. In addition, simulations were conducted to analyze how M_c changes during the progressive wetting of the layered soil. For that purpose, a new model was developed for M_c . This model also includes a sub-model for the shear mechanical strengths of the sandy soil layers and their variation with soil water content. The model was calibrated with different data sets: (1) the M_c -data obtained from the tree pulling experiments performed on 14 years-old *Pinus pinaster*; (2) the 3D root system architectures of the pulled trees ; and (3) the soil shear

*Corresponding Author.
Tel.: +33 (0)5 57 12 23 64.
Email address: pauline.defossez@inrae.fr (P. Défossez)

19 mechanical strength as function of the soil water content measured in labora-
20 tory by direct shear tests and soil water retention curve measurements. After
21 calibration, M_c -calculations were performed when simulating a progressive soil
22 wetting by water table increase or by water saturation front progression.

23 *Results.* Field-data and simulations show that M_c depends little on soil water
24 content outside the domain of complete soil saturation. Close to saturation,
25 simulations show that M_c decreases drastically up to % 40 of its value. This is
26 specific to sandy soil whose mechanical strength is mainly due to the capillarity
27 forces between grains. As illustrated by simulations, the anchorage resistance
28 results from two components. The first friction component slightly increases
29 with soil water content. The second suction component decreases little with soil
30 water content and drops down at saturation when all the interstitial water in
31 the soil porous network merges.

32 *Conclusions.* This loss of anchorage resistance at full saturation may increase
33 considerably the risk of wind damage of forest growing in sandy soil as floods
34 increase with climate change in Europe.

Keywords: Windstorm damage, Toppling, Soil water content, Anchorage, Soil
shear strength, Pinus pinaster, sandy soil

35 1. Introduction

36 Wind damage represents more than 50% by timber volume of the forest
37 damage in Europe (Schelhaas, 2008). Storm damage has considerable conse-
38 quences for the forest economy, and the ecological functioning and survival of
39 European forests (Lindroth et al., 2009; Seidl et al., 2014). The increasing stock
40 and average age of European forests and the observed on-going climate changes,
41 with the prediction of stronger wind storms (Della-Marta and Pinto, 2009), can
42 also lead to a growing wind risk. For instance, storm Klaus which hit southern

Europe in January 2009 resulted in an estimated 43 million m³ of timber being blown down in Southwest France, including a volume of 37 million m³ for *Pinus pinaster* (GPMF, 2011). In Europe, most of the damage are from tree overturning (Gardiner et al., 2016).

Different authors suggested that soil properties can impact the tree anchorage (Coutts, 1986; Ennos, 2000; Dupuy et al., 2007; Gardiner et al., 2010, 2016). The soil texture (clay or sandy soil) was established to be an important factor (Moore, 2000; Nicoll et al., 2006). With climate change, storms tend to be accompanied by heavier rainfall in Europe leading to more saturated soils (Stocker et al., 2014) with possible higher risk of wind damage. But to date, data on these effects remain scarce. Only Kamimura et al. (2012) investigated the stability of 30 year old hinoki trees under various irrigation treatments to recreate the soil conditions during typhoon. They found that high soil water content below the soil-root plate tends to decrease the tree stability. Kamimura et al. (2012) did not establish an explicit relation with the soil mechanical strength so that the role of the soil water content has not yet been clarified.

The soil shear mechanical properties of the rhizosphere have been extensively analyzed in the context of slope stability with vegetation (Stokes et al., 2008; Genet et al., 2008; Schwarz et al., 2010; Genet et al., 2010; Wu, 2013). The decrease in soil shear strength with rainfall-induced wetting has been largely recognized to trigger soil slope sliding. Numerous authors took into account for this phenomena to predict slope stability as function of climate conditions (Simon and Collison, 2002; Osman and Barakbah, 2006; Pollen, 2007; Fan and Su, 2009; Rahardjo et al., 2014; Veylon et al., 2015; Gonzalez-Ollauri and Mickovski, 2017; Yang et al., 2017; Hales and Miniati, 2017; Kim et al., 2017). This assumption was extended to the problematic of tree stability under wind and it is generally accepted that soil wetting decreases the tree anchorage strength

70 and the tree stability (Coutts, 1986; Ennos, 2000; Moore, 2000; Gardiner et al.,
71 2010, 2016).

72 Most of knowledge about the role of the soil mechanical strength on the
73 tree anchorage has come from numerical studies. Following the pioneer work of
74 Blackwell et al. (1990), numerical models have been developed to estimate the
75 tree resistance to overturning (Dupuy et al., 2005; Rahardjo et al., 2009; Yang
76 et al., 2014, 2018). Models based on the finite element method (FEM) describe
77 independently the root architecture as a ramified structure of beams and the soil
78 as a continuous medium defined by the laws of soil mechanics. Interestingly, they
79 provide a method to differentiate the effects caused by the root architecture from
80 those caused by the soil resistance. Parametric studies with FEM models were
81 conducted to examine the impact of soil shear properties on the tree stability
82 (Yang et al., 2018; Dupuy et al., 2005, 2007; Rahardjo et al., 2009). In these last
83 numerical studies, the laws used for soils do not account for soil water. Only few
84 authors examined the effect of change in soil water content on the tree stability.
85 Rahardjo et al. (2009) and Rahardjo et al. (2017) proposed to account for the
86 influence of soil hydrology for clay soils and predicted a systematic decrease
87 in tree anchorage with an increase in the soil wetting. These last simulations
88 were not corroborated by observations. In addition all these numerical studies
89 describe ideal soils or simplified root system where the interaction between roots
90 and surrounding soil are highly simplified.

91 The goal of this paper is to better understand the role of the soil mechanical
92 strength on the tree anchorage and how it changes with soil water content. We
93 focus on *P. pinaster* cultivated on a sandy soil that is representative of the
94 Landes de Gascogne Forest (France). The Landes de Gascogne Forest covers
95 1 million hectares in south-western France and has been heavily damaged by
96 winter windstorms over the last 20 least years. This study investigates changes

in the tree anchorage of young *P. pinaster* with soil wetting induced by rainfall. Our approach combines field-data and simulations to better understand the evolution of the tree stability with the progressive redistribution of water within the different soil horizons :

1. field pulling experiments were performed to measure the tree anchorage resistance in wet and very wet soil conditions;
2. a new anchorage model was developed including a detailed description of the root system properties and the soil properties in the different soil horizons. We implemented in this model a sub-model dedicated to evaluate the soil mechanical strength as a function of the distribution of water between soil horizons. This new model allows for simulating the tree resistance to uprooting in situations where all soil horizons reach saturation when experiments are technically difficult to be conducted.
3. different simulations of the tree anchorage resistance were performed as the soil layers become saturated with soil wetting. Prior simulations, the model was calibrated from (i) the field tree pulling-data (ii) laboratory-data for the 3D root system architecture of the pulled trees (iii) laboratory-data for the soil shear mechanical properties as function of the soil water content corresponding to the field pulling experiment.

2. Materials and Methods

2.1. Field-data for the tree resistance to overturning

Site description. The experimental site is located in the Landes de Gascogne Forest (Nézer forest in the southwest of France, altitude 15 m, latitude $44.6448^{\circ}N$, longitude $-1.03333^{\circ}W$; city of Teich). The site is a medium humid sandy spodosol with a discontinuous deep hard pan at 40-90 cm depth (Augusto et al.

2010). Topography is flat (average slope less than 2%). The climate is temperate marine, with moderately warm summers and cool wet winters. Mean annual rainfall is 945 mm, mean annual temperature is 13.8°C , and prevailing winds and storm winds come from the West (Météo France – 1981-2010). The water table fluctuates close to the soil surface during rainy winters, but sinks to 1.5 m depth in late summer. A major storm damaged the stands on 23 January 2009 with 18% toppled in the seeded stand and 30% in the planted stand. 12 straight trees (6 were seeded and 6 were planted) with the same development stage and without any stem fork were selected. Stem Diameter at Breast Height (DBH) varied between 16.23 and 19.09 cm and height between 9.38 and 11.65 m (Table 1). These trees represent a subsample of the 48 trees studied by Danquechin Dorval et al. (2016) who established their 3D root system architecture as detailed in the following.

Soil type. The soil of the experimental site was characterized by its particle size distribution (Figure 1). This distribution was performed on three samples by sedimentation and sieving to determine the particles diameters D_{10} , D_{50} , D_{60} corresponding respectively to 10%, 50% and 60% of passing. Soil foundation was composed of medium sand with a median particle size $D_{50}=0.40$ mm and a coefficient of uniformity $C_u = D_{60}/D_{10}=3$. The grains shape was characterized as rounded particles with medium sphericity and the fine content less than 5%. Soil particle density $\rho_s=2.60$ Mg m $^{-3}$ was measured for each horizon (0-10, 10-40 and 40-60 cm) by water Pycnometer following the procedure ASTM D 854 – 02. The loosest and densest state of the soil were characterized by the maximum e_{max} and minimum e_{min} void ratios with $e=\frac{\rho_s}{\rho_d} - 1$, ρ_d being the soil dry bulk density. $e_{min}=0.50$ and $e_{max}=0.85$ were estimated from D_{50} based on published formula (Cubrinovski and Ishihara, 2002; Patra et al., 2010). The total carbon content was measured by dry combustion in a CHN autoanalyser

149 (Carlo Erba NA 1500). The organic carbon content varied from 2.5 to 1% with
150 soil horizon depth (0-10 to 40-60 cm).

151 *Field pulling tests.* In order to measure the effects of soil water content on the
152 tree overturning resistance, pulling tests were performed at two contrasted soil
153 water content conditions. A first series of tests was performed in April 2012
154 during a period of rain with a water table at about 60 cm depth. In this series,
155 three soil horizons (0-10, 10-40 and 40-60 cm) were wet and unsaturated. A
156 second series was performed in February 2013 after a period of heavy rain with
157 a water table around 40 cm. In this second series, both first horizons were very
158 wet and unsaturated and the horizon (40-60 cm) was saturated .

159 The procedure for the tree pulling experiments was based on Nicoll et al.
160 (2006) and depicted in Fig. 4. In 2012 (04/23 and 04/24) and in 2013 (01/30
161 and 02/01) 12 trees were pulled until failure. The tops of the trees were removed,
162 leaving 3 m high stem to eliminate the contribution of the crown load (Coutts,
163 1986). The selected trees were pulled with a motorised winch (Winchmax, UK,
164 maximal strength capacity 58 kN). The winch was attached to the base of an
165 anchoring tree at a distance to the winched tree (8 to 10 m) and anchored
166 within the soil by two piles dug over a depth of 0.8 m. The height (L) of
167 the cable attachment was low enough on the stem to induce anchorage failure
168 without stem breakage. L varied from tree to tree, from 1.4 m to 1.8 m. The
169 cable attachment was guyed by screws driven through the stem to avoid the
170 slip during pulling tests. Trees were winched perpendicular to tree row lines,
171 planted trees toward East and seeded trees toward North. The pulling force
172 F applied to the winched tree was measured by a load cell (SM 5420, Sensel,
173 France, maximum load 50 kN). Two inclinometers (SN 25276; Sensel, France)
174 were tied to the tree at the cable attachment point and at the base of the stem
175 to measure respectively the tree total rotation α and the rotation of the root-soil

176 system α_r . The load cell and the inclinometers were connected to a computer
 177 that recorded data. Both the distance between the tested tree and anchoring
 178 point and the distance between the anchoring point and the cable attachment
 179 point were measured to estimate θ the angle of the cable from the horizontal.

180 The turning moment M applied to the tree by the winching apparatus was
 181 calculated as followed :

$$M = FL(\cos \theta \cos \alpha + \sin \theta \sin \alpha). \quad (1)$$

182 We estimated from the $M(\alpha_r)$ curves: (i) the initial stiffness of the root-soil
 183 system k_r , deduced from the initial linear part of the moment-rotation curves
 184 (Neild and Wood, 1999; Jonsson et al., 2006; Lundström et al., 2007), (ii) the
 185 critical turning moment M_c , corresponding to the maximum of the moment-
 186 rotation curves, (iii) the critical angle α_r^c corresponding to M_c . M_c characterizes
 187 the tree capacity to resist overturning induced by windstorms (Coutts, 1986).

188 *Field soil water content conditions.* The degree of soil saturation during pulling
 189 tests were deduced from the measurements of the soil gravimetric water content
 190 w_n and the soil dry bulk density profiles ρ_d as function of soil depth z . Both
 191 w_n and ρ_d were measured by gravimetric method on samples collected the same
 192 day as the pulling experiments. Soil samples were collected by cylinders at 5, 20
 193 and 45 cm depth from soil surface in 2012 and at 5 and 20 cm in 2013. In 2013,
 194 it was impossible to collect cylinders at larger depth because of soil saturation.
 195 Cylinders were of 8 cm height and 5 cm diameter. Four profiles were measured
 196 for each tested tree at four points of the compass, at 2 m from the tree stump
 197 to capture variability of the soil water content. The saturation degree S_r was
 198 deduced as follows:

$$S_r = w_n \frac{\rho_s \rho_d}{\rho_w (\rho_s - \rho_d)} \quad (2)$$

199 with ρ_w the water density.

200 *Root system characteristics.* The analysis of the 3D architecture root systems
201 of the 12 tested trees has been presented in Danquechin Dorval et al. (2016).
202 Root systems were excavated on 15 May 2012 for the first 6 pulled trees and on
203 the 25 February 2013 for the others. Roots were classified in Fig. 3 according
204 to their orientation and position in space. The taproots (T) follow vertical
205 direction and the shallow roots follow horizontal direction and differ if they are
206 in the winch sector (W) or in the counter-winch (CW). In this study, the roots
207 are quantified by their volume V_{root} and by their specific root length (SRL)
208 defined as the ratio between root length and root volume without stump. The
209 finer are roots, the higher SRL is. SRL -values were corrected to avoid a bias
210 due to root end loss during excavation (Danquechin Dorval et al., 2016).

211 2.2. Model for the tree resistance to overturning

212 The purpose of this section is to describe the tree resistance to overturning
213 with a model that accounts for the soil mechanical properties and their variation
214 with the soil water content.

215 *Anchorage rupture.* This model is based on the observations of overturning
216 performed during the pulling tests. Usually, for large pine, the root-soil system
217 exhibits a large root-soil plate where soil is very dense and where soil is em-
218 bedded in a root cage (Danjon et al., 2005). Large trees present a massive and
219 dense root-soil plate that tilts as a block during the overturning failure. For
220 smaller trees, like those studied here, there is no such a cage (Danquechin Dor-
221 val et al., 2016). Here, the winching tests showed that failure occurs by mixed
222 mode of ruptures: the ruptures of roots them-self usually by delamination and
223 by progressive pullout of the flexible roots (Figure 2).

224 A simplified model representative of the observed failure modes was estab-
 225 lished by considering that each root i develops a moment m_i with one component
 226 related to the root strength (m_{root}^i) and the other related to its interaction with
 227 the surrounding soil ($m_{root/soil}^i$). The total resisting moment results from the
 228 sum of the resistance of the N roots:

$$M(\alpha_r) = \sum_{i=1}^N m^i(\alpha_r) = \sum_{i=1}^N [m_{root}^i(\alpha_r) + m_{root/soil}^i(\alpha_r)]. \quad (3)$$

229 At failure, when the root system rotation α_r reaches the critical rotation α_r^c ,
 230 the critical resisting moment can be written :

$$M_c = M_c^{root} + M_c^{root/soil}. \quad (4)$$

231 The root component M_c^{root} contributing to the critical resisting moment can
 232 be expressed as follows :

$$M_c^{root} = \sum_{i=1}^N l_i a_i \sigma_{root}^i, \quad (5)$$

233 where σ_{root}^i is the root strength, a^i is the section area of the root i and l_i
 234 the lever arm of the resulting force (Fig. 4). The contribution of both mode
 235 of resistance to the critical turning moment, either by root strength or soil-root
 236 friction, is expected to depend on root size. The rupture threshold is given by
 237 the weakest component either the root or the root-soil interface breaking first.
 238 For small structural roots, the failure threshold will be mostly given by the root
 239 strength (σ_{root}^i). On the contrary, large roots are more resistant so that failure
 240 will occur preferentially at the soil-root interface.

241 The root/soil interface component $M_c^{root/soil}$ can be expressed as follows:

$$M_c^{root/soil} = C_0 + \frac{1}{S} \sum_i l^i S^i \tau_f^i, \quad (6)$$

242 with τ_f^i the average soil shear strength. S^i is the external surface of the root
 243 i and S is the total external surface of the root system. The term C_0 is a con-
 244 stant factor introduced to consider the possible interaction between roots. The
 245 complete development of the resistance of each root requires the mobilization of
 246 a certain volume of soil surrounding the root corresponding to its zone of influ-
 247 ence. The proximity of the roots of each other within the root system leads to
 248 arching effects within the soil between the roots, and may result in a positive or
 249 negative contribution depending on the root system architecture (root diameter,
 250 spacing, connectivity, etc.), reflecting by C_0 . This architectural mechanism has
 251 been studied extensively for pile groups (Patra et al., 2010; Shanker et al., 2006;
 252 Vanitha et al., 2007; Shelke and Patra, 2008) in the geotechnical engineering
 253 field.

254 *Influence of soil water content.* The root/soil interface component $M_c^{root/soil}$ is
 255 expected to vary with the soil water content in relation to τ_f^i . According the
 256 mechanics of unsaturated soils (Fredlund et al., 1978; Gan et al., 1988; Guan
 257 et al., 2010), each τ_f^i can be decomposed in a frictional τ_φ^i and suction component
 258 τ_ψ^i :

$$\tau_f^i = \tau_\varphi^i + \tau_\psi^i. \quad (7)$$

259 Then the root/soil interaction component of the critical resisting moment be-
 260 comes:

$$M_c^{root/soil} = C_0 + M_\varphi + M_\psi, \quad (8)$$

261 with $M_\varphi = \frac{1}{S} \sum_i l^i S^i \tau_\varphi$ and $M_\psi = \frac{1}{S} \sum_i l^i S^i \tau_\psi^i$. When compiling Eq. 5 and Eq.
 262 8, the critical resisting moment can be expressed as:

$$M_c = \sum_{i=1}^N l_i a_i \sigma_{root}^i + C_0 + \frac{1}{S} \sum_i l^i S^i \tau_\varphi + \frac{1}{S} \sum_i l^i S^i \tau_\psi^i. \quad (9)$$

263 2.3. Sub-model used for the soil mechanical strength

264 A sub-model was required to describe the evolution of the soil shear strength
 265 with soil water content in sandy soils. For each soil layer, the soil shear strength
 266 was evaluated using a similar procedure as described in Veylon et al. (2015).
 267 As the soil fine content was low, effective cohesion was assumed equal to zero.
 268 Therefore, the shear strength of Eq. 6 was modeled with the following failure
 269 criterion (Oberg and Sallfors, 1997):

$$\tau_f = (\sigma_n + S_r \psi) \tan \varphi_p, \quad (10)$$

270 where σ_n is the mean net vertical stress applied within each soil layer, φ_p its
 271 peak friction angle (deg.) at saturation, S_r its saturation ratio $S_r = w_n / w_{sat}$ with
 272 w_{sat} , the soil gravimetric water content at saturation and ψ its matric suction.
 273 Both terms $\sigma_n \tan \varphi_p$ and $S_r \psi \tan \varphi_p$ correspond respectively to the frictional
 274 component (τ_ϕ) and to the suction component (τ_ψ) of the shear strength (τ_f) ac-
 275 cording to Eq. 7. The frictional component mainly depends on the soil porosity
 276 and on the mean effective stress as detailed in the following paragraph and in-
 277 creases with soil water content. The suction component due to the development
 278 of capillarity forces between soil grains decreases with soil saturation ratio.

279 The peak friction angle φ_p in the frictional component was estimated for
 280 each soil layer to account for its dependency on both the soil porosity and the
 281 pressure. It is well known that φ_p depends on the sand state (Been et al., 1991;
 282 Bolton, 1986) and that φ_p is not constant under very low pressure (< 20 kPa)

283 (Fukushima and Tatsuoka, 1984; Tatsuoka et al., 1986; Baker, 2004; Fannin
 284 et al., 2005; Chakraborty and Salgado, 2010; Rouse, 2018). This phenomenon
 285 is attributed to the effect of dilatancy and can be modeled with the relative
 286 dilatancy index I_R following the stress-dilatancy theory (Rowe and Taylor, 1962;
 287 De Josselin De Jong, 1976; Bolton, 1986). To account for these effects, φ_p
 288 was estimated as a function of both the mean effective pressure p' and the
 289 void ratio e with $p' = \sigma_n(1 + 2K_0)/3$, K_0 is the horizontal earth pressure at
 290 rest, approximated here by $K_0 = 1.15 - \sin \varphi_c$ (Llano-Serna et al., 2018). The
 291 relationship used for φ_p was:

$$\varphi_p = \varphi_c + A_\Psi I_R, \quad (11)$$

292 where φ_c and A_Ψ are two constant parameters. The term I_R depends on p' and
 293 e as follows:

$$I_R = I_D(Q - \ln p') - 1. \quad (12)$$

294 Here, the term Q depends on p' while I_D depends on e . Q is a parameter that
 295 depends on the intrinsic sand characteristics and was estimated by the relation
 296 proposed by Chakraborty and Salgado (2010) based on a large database of
 297 experimental results on clean sands:

$$Q = 7.1 + 0.75 \ln p'. \quad (13)$$

298 I_D is the relative density of the soil defined:

$$I_D = \frac{e_{max} - e}{e_{max} - e_{min}}. \quad (14)$$

299 *2.4. Simulating the tree resistance to overturning for different soil water condi-*
300 *tions*

301 The possible effect of soil wetting on the critical resisting moment M_c (Eq.
302 9) was examined by simulating two saturation scenarios.

303 The first scenario consists in increasing the water table level. Such a rise
304 in the water table level may be caused by continuous rainfall during a certain
305 period of time (e.g. during winter). The model assumes that the soil profile
306 is separated into a saturated zone under the water table level ($S_r = 1$) and an
307 upper unsaturated zone ($S_r < 1$). Three different values of water table level are
308 considered $\mathcal{WT} = -0.1$ m, -0.4 m and -0.6 m. Under the water table level, the
309 soil is considered as saturated and above the water table level, the soil has a
310 variable saturation degree S_r .

311 The second scenario corresponds to the downward progression of a saturation
312 front level. This case may occur according to infiltration mechanism in case of
313 heavy rain concentrated in time. The model used for this scenario is the Green-
314 Apmt model (Green and Ampt, 1911) widely used in water resources research
315 field (Chen and Young, 2006; Kale and Sahoo, 2011). This model assumes a
316 homogeneous soil profile and an uniform distribution of the initial saturation
317 ratio. A saturation front separates the soil profile into an upper saturated zone
318 ($S_r = 1$) and a lower unsaturated zone where the saturation ratio of the soil
319 stays at its initial value ($S_r < 1$). Despite its simplicity, the Green-Ampt model
320 provides a reasonably accurate estimate of the infiltration front evolution which
321 is sufficient for most of the field problems (Whisler and Bouwer, 1970; Gill,
322 1978; Dagan and Bresler, 1983; Govindaraju et al., 1992; Kargas and Kerkides,
323 2011). Three different values of saturation front level are considered $\mathcal{SF} = 0.0$
324 m, -0.1 m and -0.4 m. Above the saturation front level, the soil is considered as
325 saturated and bellow the saturation front level, the soil has a variable saturation

326 degree S_r .

327 2.5. Main hypothesis for model parametrization

328 The parameters used for the root dimensions came from the root architecture
329 measurement and those for the soil strength from soil mechanical tests and
330 soil-water retention measurements (following section 2.6) . Then, the other
331 unknown parameters, M_0 and l_i , were estimated by fitting the field data critical
332 turning moment M_c -data with the expression proposed for the tree resistance
333 to overturning (Eq. 9).

334 These parameters estimations were based on different hypothesis:

- 335 • σ_{root}^i was assumed not to depend on its diameter in agreement to Genet
336 et al. (2005) for roots higher than 2 mm;
- 337 • a_i was assumed to be proportional to S_i with S_i estimated from SRL
338 ($S = 1/SRL$). SRL -values were estimated from the 3D-root architecture
339 by grouping the roots according to the sector and the type they belong
340 to : winching shallow root (S_W), counter winching shallow root (S_{WC}) or
341 tap roots (S_T). The contribution of sinker roots to M_c was neglected;
- 342 • the surrounding soil was decomposed in three layers corresponding to 0-
343 10 cm, 10-40 cm and 40-60 cm depths. The variation in the organic carbon
344 content with soil depth was neglected. The effect of the tree weight was
345 also neglected. Then the critical shear strength parameters only depended
346 on the ρ_d and w_n values of each layer as previously described (section 2.3);
- 347 • the shallow roots develop mainly between 10 and 40 cm depth (Fig. 3).
348 Then the shear strengths surrounding the shallow roots were estimated in
349 the middle of the 10-40 cm from the measurement of the shear strength
350 τ_f^{10-40} . Similarly the measurement τ_f^{40-60} were used to estimate the soil
351 shear strengths surrounding the tap roots.

352 According to these hypothesis and Eq. 9, the expression for the critical
 353 resisting moment M_c was as follows:

$$M_c = M_0 + M_k^{10-40} + M_T^{40-60}, \quad (15)$$

354 with

$$M_k^{10-40} = \frac{S_k}{S} (l_k^\varphi \tau_\varphi^{10-40} + l_k^\psi \tau_\psi^{10-40}), \quad (16)$$

355

$$M_T^{60-40} = \frac{S_T}{S} (l_T^\varphi \tau_\varphi^{40-60} + l_T^\psi \tau_\psi^{40-60}), \quad (17)$$

356 where $k=W$ or WC . M_0 is a constant with $M_0 = C_0 + \sum_{i=1}^N l_i a_i \sigma_{root}^i$. l_W^ψ , l_{WC}^φ ,
 357 l_{WC}^ψ , l_T^φ , l_T^ψ are constant parameters representing equivalent lever arms. These
 358 parameters are expected to be of the order of meters and can be positive or
 359 negative as they have favourable or unfavorable effect on the resisting moment.
 360 The lever arms coefficients l_i and M_0 were determined by multi-linear regression
 361 of the field M_c -data.

362 Once the parameters were estimated, the critical resisting moment M_c was
 363 calculated from Eq. 15 for both scenarios for which we considered a tree with
 364 the average characteristics (SRL , S_W , S_{WC} and S_T) measured for the 12 trees
 365 (Table 1).

366 2.6. Model parameters for the soil sub-model

367 For both simulated scenarios, the soil shear strengths for 10-40 and 40-60
 368 and their variation with the soil layer water content were estimated from Eq.
 369 10 for a range of saturation ratio between 0.1 to 1.

370 *Net vertical stress σ_n .* The net vertical stress σ_n was estimated at the middle
 371 of each layer, i.e. at 25 cm and 50 cm depths. We assumed that the weight
 372 of the tree can be neglected as regards to the vertical pressure induced by the

soil overlying layers. Therefore, the net vertical stress only depends on the soil porosity and water contents of the soil overlying layers.

Matric suction ψ . Matric suction ψ were deduced from the water retention curve $S_r(\psi)$, estimated from soil-water retention measurements by considering a unique matric suction curve for both soil layers (10-40 or 40-60).

The water retention curve was determined using pressure plate method (Richards, 1941) from soil samples collected in the field site at 0-10, 10-40 and 40-60 cm. The pressure plate device consists of a pressure vessel which can be pressurised up to a air pressure of 1500 kPa. Soil samples were placed on a ceramic disc that has a specified air entry pressure value. The disc was connected to the atmosphere and water is allowed to flow out freely. Pressure steps were applied by a flow control valve and controlled by a pressure gauge. During the whole test, the temperature in laboratory was controlled at around 20 °C. In order to determine the balance time under each pressure, the samples were removed and weighted using electronic scales having accuracy of 0.01 g every 12 h for each pressure step. If the mass of the sample remained unchanged after 24 h, then it was assumed to be in a state of equilibrium and the gravimetric water content was measured.

Samples per soil horizon were packed at $\rho_d = 1.23, 1.41, 1.58 \text{ Mg m}^{-3}$ for respectively soil layers 0-10, 10-40 and 40-60 cm in cylinder of 3.4 mm diameter and 1.9 mm height. These ρ_d -values corresponded those of the field pulling tests. Five air pressures were applied to three samples per soil horizon corresponding to matric suction equal to 1, 3.2, 10, 32 and 100 kPa.

The matric suction ψ was estimated from the saturation ratio S_r by modeling the soil-water retention curve-data (Fig.5). Over the years, a number of water retention curves have been proposed (Fredlund and Xing, 1994). The best fit to our experimental data was obtained using the model developed by Lebeau and

400 Konrad (2010) and validated by Konrad and Lebeau (2015). This model is not
 401 purely empirical but explicitly accounts for the mechanisms of water retention
 402 (capillarity and adsorption):

$$S_r = S_{rc} + (1 - S_{rc})S_{ra}, \quad (18)$$

403 with

$$S_{rc} = \begin{cases} 1 & \psi \leq \psi_a, \\ 1 - (1 - e^{-\Lambda\psi})^\zeta & \psi > \psi_a, \end{cases}$$

404

and

$$S_{ra} = S_{ro} \left(1 - \frac{\ln \psi}{\ln \psi_d}\right)$$

405 In this expression, S_{rc} describes the effect of the capillary forces and S_{ra}
 406 the effect of the adsorptive forces. The parameters ζ and Λ are shape and scale
 407 parameters of the pore-size distribution, respectively. $\psi_a = \psi_d^{1-1/S_{ro}}$ is the
 408 matric suction for which the degree of saturation due to adsorption reaches 1,
 409 S_{ro} is the degree of saturation due to adsorption at a matric suction of 1 kPa
 410 and ψ_d is the matric suction at oven dryness, which is approximately 10^6 kPa.
 411 The parameters of the soil-water retention curve (Eq. 18) were determined by
 412 minimizing the square error between the calculated and measured saturation
 413 ratios. They were found equal to $S_{ro} = 0.11$, $\zeta = 0.62$ and $\Lambda = 0.49$ ($R^2 = 0.86$).
 414 The adjusted water retention curve is represented on Fig.5.

415 To estimate the matric suction ψ , an approximation for the expression Eq.
 416 18 was used in the range $S_r = 0.1 - 1.0$ where the capillary component is
 417 predominant:

$$\psi = -\frac{1.30}{\Lambda} \ln \left(1 - (1 - S_r)^{1/\zeta}\right). \quad (19)$$

418 Eq. 19 was used to estimate ψ as function of S_r in the expression used to
 419 evaluate soil shear strength (Eq. 10).

420 *Peak friction angle φ_p .* The peak friction angle φ_p was estimated for each soil
 421 layer (10-40 or 40-60) using direct shear tests. These laboratory tests were
 422 performed for both layers 10-40 and 40-60 for soil samples at different initial
 423 void ratio e , different net vertical stress σ_n and different saturation ratio S_r .
 424 Combined with the $S_r(\psi)$ curve, these tests allowed for estimating φ_c and A_ψ
 425 of the peak friction angle φ_p (Eqs.11-14).

426 Direct shear tests were conducted using a Wykeham Farrance shear testing
 427 machine to characterize the soil mechanical properties. Soil samples were col-
 428 lected at two horizons 10-40 and 40-60 cm depth in the field site. Soils were
 429 air dried and sieved through <2 mm. Soil samples were packed at two porosity
 430 corresponding to the dry bulk density ρ_d of 1.41 and 1.58 Mg m⁻³ of the soil of
 431 layers 10-40 and 40-60 cm for the 12 pulled tree locations. Four initial gravi-
 432 metric water contents were tested: $w_n = 0.1, 0.15, 0.2$ and soil saturation. For
 433 unsaturated soil samples ($w_n=0.1$ to 0.2), soils were obtained by spraying dried
 434 sieved soils with water until the desired water content was reached, and then
 435 the specimens were compacted in cylinder at the desired initial bulk density.
 436 For saturated conditions, specimens were first packed in cylinders with soil at
 437 $w_n=0.1$ to obtain the initial desired bulk density. After sample preparation,
 438 the specimens were kept in airtight containers at 4°C for at least 24 hours be-
 439 fore being sheared (Oloo and Fredlund 1996). This duration was considered
 440 sufficient to ensure the equilibrium of air and water in the specimens (Wen
 441 and Yan, 2014). Then, the specimens were saturated directly in the shear cell
 442 following the procedure ASTM D 3080-90. The lateral displacement rate was
 443 0.38 mm/min compatible with drained conditions. Each direct shear test pro-
 444 vided one soil response curve relating the shear stress (τ) to the lateral relative
 445 displacement (δ) for four net vertical stress $\sigma_n = 3.17, 6.01, 8.05$ and 13.56 kPa.

446 The constant parameters φ_c and A_ψ of the peak friction angle φ_p (Eqs.11-

14) were estimated from the φ_f -data. The stress-displacement response of each soil sample was analyzed individually to determine the pertinent values of shear strength (τ_f). The shear strength was determined as the maximum value of shear stress measured during the shear loading. When no peak value or plateau was observed, the test was rejected. The results for tests in saturated conditions are presented in Table 4. The values of φ_c and A_Ψ were determined by minimizing the square error between the τ_f -data measured for 10-40 and 40-60 and the calculation of τ_f obtained using Eq. 10 with σ_n the vertical stress applied during the direct shear tests and ψ the value calculated with Eq. 19 from the saturation ratio of the soil sample.

3. Results

3.1. Variations in the field the critical moment with soil water content

The overturning moment M is presented for the 12 trees in Fig.6 according to the rotation of the root-soil system α_r . The response curves $M(\alpha_r)$ exhibited typical elasto-plastic material behavior with a linear part at small angle and a transition to elasto-plastic range. The curve reached a maximum M_c that can be considered as the ultimate rupture of the soil-root system. The decrease in resisting moment was due to root breakages and pullout: the lateral roots were stretched and failed one after the other both in the counter winchward and in the winch ward side, the taproot failed by flexion or delamination (pictures not shown). Few $M(\alpha_r)$ curves exhibited oscillations during pulling, probably due to successive failures as the root slid (Fig. 6).

The tree anchorage resistance varied from 7.92 to 16.10 kN.m between the 12 trees (Table 2). Similarly the root-soil stiffness k_r varied among specimens between 1.69 and 3.91 kN/m/°. M_c was positively and linearly correlated to k_r

472 with $M_c = 0.24k_r$ ($R^2=0.69$, $P<0.001$), showing that the most flexible root-
473 system had the lowest rupture strength.

474 The soil water conditions for tree pulling were different in the two series. The
475 mean soil water contents were 0.13 and 0.24 $\text{g}\cdot\text{g}^{-1}$ for the first and the second
476 series respectively and were significantly different using student-tests (Table 2).
477 Note that this last value corresponds to measurements for only 2 depths (5, 20
478 cm) because of soil saturation at higher depth. In terms of soil saturation, the
479 saturation ratio of the three soil layers in the first series ranged from $S_r=0.098$
480 to 0.182 whereas the minimum of S_r was 0.152 and all the 40-60 layers reached
481 saturation ($S_r \approx 1$) in the second series.

482 Significant correlation was found between M_c -values and variables describing
483 the root architecture, in particular $R=0.88$ ($P<0.001$) with the total volume of
484 roots and $R=-0.85$ ($P<0.001$) with the total SRL (Table 3). On the contrary,
485 the variations in ρ_d and w_n between trees and between series did not explain
486 the M_c variations as no statistical correlation was found with these factors.

487 3.2. Estimation of soil shear strength using the soil sub-model

488 The shear strength τ_f deduced from the soil sub-model (Eq. 10) are com-
489 pared to the measurements in Fig.8. τ_f -calculations are based on the constant
490 parameters φ_c and A_Ψ of the peak friction angle φ_p (Eqs.11-14). The opti-
491 mal value for φ_c was $\varphi_c = 34^\circ$, which is coherent with the nature of the soil
492 (Sadrekarimi and Olson, 2011). The optimal value $A_\Psi=3.7$ was obtained and
493 lies in the interval 3-5 of the admissible values (Bolton, 1986).

494 The correlation between τ_f -calculation and τ_f -measurement is $R^2 = 0.80$ and
495 the predictive model error is less than 2 kPa, which is acceptable as regards to
496 the expected in situ variability of soil properties, in particular the retention curve
497 (Zapata et al., 2000) (Fig. 5). This illustrates the ability of the soil sub-model
498 to predict with a reasonable accuracy the shear strength of the unsaturated soils

499 interacting with the tree root systems.

500 3.3. Modelling the critical moment

501 The parameters of the M_c -model (Eq. 15) as estimated by multi-linear
502 regression analysis of the M_c -data for the 12 tree specimen are presented in
503 Table 5. The parameters l_i^j can be viewed as equivalent lever arms and reflect the
504 contributions of the soil-root interactions to the resisting moment in each root
505 sector. Their values are positive for all sectors (from 1.12 to 9.69 m) reflecting
506 a favorable effect of the soil on the resisting moment, except for the roots in
507 the counter winch sector where the value is -0.32 for the frictional component
508 l_{wc}^φ . The comparison between the measured resisting moment and the resisting
509 moment predicted by the model (Fig. 9) show that the predictive capacity of
510 the model is fairly good ($R^2=0.90$ and $SE=0.8$ kN.m). The maximum relative
511 error remains below 10% of the measured resisting moment which is low in
512 comparison to the field variability measured for the root systems and for the
513 soil layers (Tables 1 and 2).

514 3.4. Simulations of the tree resistance with soil saturation

515 *Increase of the water table level.* The first scenario simulates an increasing water
516 table level \mathcal{WT} from -0.6 m to -0.1 m. The evolution of the critical turning
517 moment with the saturation ratio above the water table level is presented in
518 Figure 10. It represents how M_c changes with the progressive wetting of the top
519 soil horizon until the complete saturation of all the soil layers. For all water table
520 levels, the critical turning moment slightly increases with saturation ratio. In the
521 quasi-saturated domain, which is assumed to be reached for $S_r \geq 0.95$ (Monnet
522 and Boutonnier, 2012), the curves abruptly collapse as the medium becomes
523 quasi-completely saturated because the interstitial water porous network merges
524 and the water can transmit pressure within the whole fluid phase.

525 *Progression of a saturation front.* In the second scenario, the rainfall induced
 526 a downward progression of a saturation front level (\mathcal{SF}). The evolution of the
 527 critical turning moment with the saturation ratio above the water table level
 528 is presented in Figure 11. It simulates how M_c changes as the lower layer
 529 wetting until full saturation. For all saturation front levels and S_r less than
 530 0.20, the critical turning moment increases as the saturation ratio increases.
 531 Then, for higher values of saturation ratio and $\mathcal{SF} = 0.0$ m and -0.4 m, M_c
 532 slightly decreases with saturation ratio. In the quasi-saturated domain ($S_r \geq$
 533 0.95), the same phenomenon occurs than for previous simulations : the curves
 534 abruptly collapse as the medium becomes quasi-completely saturated. For a
 535 given saturation ratio of the soil below the saturation front, M_c decreases as
 536 the saturation front progresses with depth. The evolution of the critical turning
 537 moment is quite limited when the saturation front progresses from 0.0 m et -0.1
 538 m : M_c decreases by less than 1 kN.m for saturation ratios around 0.2-0.25. As
 539 the saturation front progresses to -0.4 m, M_c decreases as the saturation ratio
 540 increases, but the diminution does not exceed 1 kN.m.

541 4. Discussion

542 *Model parametrization and evaluation.* The new model proposed here for tree
 543 anchorage improves the description of the mechanical processes in play at the
 544 root-soil interface and their variation with soil saturation. This model contains
 545 a sub-model for the soil shear properties. This soil sub-model for sandy soils
 546 accounts for the matric suction and also considers the packing soil state through
 547 p' and e . These last two variables have been recognized key in the strength of
 548 sandy soils at low pressure (Houlsby, 1991). The anchorage model also contains
 549 a description of root system through the distribution of the root surfaces per
 550 wind sector and per soil layers. In comparison, previous numerical studies have

551 used a rough estimation of the soil mechanical properties with idealized soil
552 types (Dupuy et al., 2005; Fourcaud et al., 2007) or parameters measured at
553 high vertical pressure (Yang et al., 2014; Rahardjo et al., 2017, 2009, 2017;
554 Yang et al., 2018). When the soil hydrology was considered, the authors used
555 idealized root systems unrepresentative of the studied tree species (Rahardjo
556 et al., 2009, 2017).

557 The present model was not designed to predict the risk of overturning but
558 rather to analyze the mechanics of the root-soil system. Indeed the size of the
559 test population (12) was small in relation to the number of regression variables:
560 7 parameters to be estimated. The justification for the choice of regression
561 variables was based on mechanical considerations. In order to evaluate the sen-
562 sitivity of the regression results, we performed "leave-one-out" cross validations
563 on each test (Sammur C., 2010). We obtained 12 sets of regression coefficients
564 calibrated on 11 tests leaving one test out for validation. The values of the
565 mean and the standard error of regression coefficients obtained by the leave-
566 one-out procedure did not exhibit large discrepancy with the parameters-values
567 (Table 5). This cross validation procedure illustrates the relative robustness of
568 the developed methodology and the degree of confidence that can be placed in
569 simulations.

570 The developed methodology also appears corroborated by the parameters-
571 values themselves. The values of the lever arms are in the order of a meter, which
572 is consistent with the size of the root systems (Table1). The positive values
573 traduce the favorable contributions of the soil-root interfaces to the resisting
574 moment. The negative contribution obtained for the roots of the plate in the
575 counter winch sector could be interpreted as the effect of deconfinement of the
576 soil under roots located in the counter winch sector as the root system rotates.
577 In this sector, the roots tend to pull out during uprooting (Fig.2) thus reducing

the resistance to overturning by the root-soil complex. The more roots in this sector, the more soil deconfinement occurs.

This model is also consistent with the data of Kamimura et al. (2012) who performed tree-pulling experiments on 30 years old hinoki trees (DBH about 19 cm, $H = 16$ m) on a yellowish brown forest soil and an Andisol soil. Starting from the assumption that heavy rains during a typhoon decreases soil strength, Kamimura et al. (2012) investigated the effect of irrigation treatments on the tree stability. Kamimura et al. (2012) showed that the water content inside the soil-root plate tended to increase the tree stability. This can be interpreted by the increase of the load of the soil-root plate which corresponds in our model to the frictional component $\sigma_n \tan \varphi_p$ (Eq. 10). This last term depends on the above soil layer weight that increases with soil water content. Kamimura et al. (2012) found that the tree stability decreases with the water content below the root-soil plate. This observation is also coherent with the suction component $S_r \psi \tan \varphi_p$ of the model (Eq. 10) that increases when saturation ratio decreases with the capillarity forces between soil grains.

Understanding tree resistance to overturning as function of soil water content in a sandy soil. Our main focus was to investigate the assumption that water wetting decreases the anchorage strength by decreasing soil mechanical strength. Our finding suggest that this assessment is mitigated for sandy soils outside the full saturation conditions.

This is illustrated by our field experiment where M_c did not exhibit change with soil water wetting in the case of unsaturated soil conditions. These unsaturated soil conditions are representative of the soil conditions during windstorm in the Landes de Gascogne Forest. Until now, complete soil saturation remain rare in this area. This was evidenced by Deirmendjian et al. (2018) who reported that complete soil saturation was reached only two days over the period

2014-2015 for a young Maritime pine forest similar to the site studied here. But fully soil saturation conditions are expected to be more frequent with ongoing climate change because of the increase in the precipitation during winter when storms usually occur in Europe (Stocker et al., 2014; Gardiner et al., 2010).

Our simulations also depart from the assumption that soil rainfall-induced wetting decreases soil shear mechanical properties and thus the tree root resistance against wind storms. To date, calculations for clay soils showed that M_c was systematically lower in wetter soils (Rahardjo et al., 2009, 2017). Our simulations evidence for specificities of sandy soils.

In sandy soils, the evolution of the resisting moment with saturation ratio is not monotonous and not trivial. It depends on the distribution of the water within the tree anchoring mass. The water table level has a major influence on the evolution of the resisting moment for saturation ratio outside the quasi-saturated domain. It has an influence on the resisting moment in dry condition (above the water table level) and on the shape of the $S_r - M_c$ curve. Our analysis suggests that a sharp decrease in overturning resisting moment with the soil water content is susceptible to occur when parts of the anchoring mass of the root system reaches the quasi-saturated domain, for example when an intense rain episode occurs during a storm.

Our model allows for analyzing the different mechanical processes in play with soil wetting. Figure 12 shows the evolution of the different components of the resisting moment with the saturation ratio for a water table level $\mathcal{WT} = 0.40$ m. The component (M_0) provides the most important part of the resistance to overturning (around 65%) and does not depend on the saturation state of the soil. It represents the resistance due to each individual root (σ_{root}^i) and the global effect of root system architecture (C_0). The frictional component (M_φ) represents a shear of the order of 30% increases as the saturation ratio

632 increases. This phenomenon is due to the soil weight increase with soil water
 633 that increases the vertical stress applying to the soil-roots interface. The suction
 634 component (M_ψ) is negative and slightly decreases (less than 10%) the moment
 635 of resistance in the unsaturated domain. This can be explained by the saturation
 636 of the 40-60 cm layer and the existence of the corresponding hydrostatic pressure
 637 which level off the saturated soil layer. When the quasi-saturated domain is
 638 reached, the hydrostatic pressure is established throughout the whole soil mass
 639 and the hydrostatic pressure experiences a sudden drop of the order of 5 kPa
 640 corresponding to a hydrostatic charge of 0.5 m of water.

641 *Implications for wind risk models.* This study highlights the need to focus on the
 642 occurrence of saturation situations with high precipitations or floods to prevent
 643 wind risk for forest growing in sandy soils. More particularly, our observation on
 644 one sandy soil can be applied to the Landes de Gascogne Forest since the region
 645 has very low soil variability. The Landes de Gascogne Forest grows on podzols.
 646 The variation in texture of these soils is low and their spatial heterogeneity
 647 principally comes from the river network that induces the presence or absence
 648 of cemented horizon between 1 to 0.3 m depth corresponding to the fluctuation
 649 of the water table between winter and summer (Jolivet et al., 2007). For a
 650 perspective of preventing wind risk at regional scale, identifying and mapping
 651 the inundated areas to improve their drainage, is a first way of improvement.
 652 A second way would be to include the evolution of soil saturation in the wind
 653 risk models applied to the Landes de Gascogne Forest (Cucchi et al., 2005;
 654 Kamimura et al., 2016).

655 This study also provides observations useful for wind risk models. The over-
 656 turning stiffness of the root system k_{root} was found to be highly linearly corre-
 657 lated to M_c . Such a correlation is one of the first observation for forest trees
 658 (Sagi et al., 2019). From a practical point of view, measurements of k_{root} in-

stead of M_c could be an alternative method to avoid systematic tree damage when performing tree winching tests. Until now, wind risk models are based on numerous destructive tree pulling tests on different species and different soil conditions for estimating the anchorage resistance. This finding suggests systematically measuring k_{root} when pulling tests to establish robust relationships $M_c(k_{root})$ for different species and soils.

5. Conclusion

This study presents new insights into the soil water content influence on tree anchorage. A new model for tree anchorage was developed involving an accurate description of the soil mechanical properties and the architecture of roots. This model is generic and could be transferable to trees of various developmental stages, different species and different soils in future studies. Combined with field-data, model simulations suggest that the anchorage of young *Pinus Pinaster* in sandy soil does not decrease drastically with soil wetting until the soil reach full saturation. This finding departs from previous findings. We argue that the difference is primary due to the specificity of sandy soils. Our analysis show that complete soil saturation in sandy soil induces a considerable drop in the tree anchorage. This result could have important implication for wind risk in forests growing in sandy soils in Europe. With climate change, storms will occur with heavier rainfall leading to more saturated soils inducing a higher risk of wind damage.

Acknowledgments

The authors would like to acknowledge Dr. Sylvain Dupont for his critical readings of the manuscript. This work was financially supported by the

683 Aquitaine Region with the FAST-A project, and by the French National Re-
684 search Agency (ANR) with the TWIST (ANR-13-JS06-0006) and FOR-WIND
685 (ANR-12-AGRO-0007) projects. This study has been also carried out in the
686 framework of the Cluster of Excellence COTE (ANR-10-LABX-45).

687

688 References

689 Baker, R., 2004. Nonlinear Mohr envelopes based on triaxial data. Jour-
690 nal of Geotechnical and Geoenvironmental Engineering 130, 498–506.
691 doi:10.1061/(ASCE)1090-0241(2004)130:5(498).

692 Been, K., Jefferies, M.G., Hachey, J., 1991. The critical state of sands. Géotech-
693 nique 41, 365–381. doi:10.1680/geot.1991.41.3.365.

694 Bolton, M.D., 1986. The strength and dilatancy of sands. Géotechnique 36,
695 65–78. doi:10.1680/geot.1986.36.1.65.

696 Chakraborty, T., Salgado, R., 2010. Dilatancy and shear strength of sand at
697 low confining pressures. Journal of Geotechnical and Geoenvironmental En-
698 gineering 136, 527–532. doi:10.1061/(ASCE)GT.1943-5606.0000237.

699 Chen, L., Young, M.H., 2006. Green-Ampt infiltration model for sloping sur-
700 faces. Water Resources Research 42. doi:10.1029/2005WR004468.

701 Coutts, M.P., 1986. Components of tree stability in sitka spruce on peaty gley
702 soil. Forestry 59(2), 173–197. doi:10.1093/forestry/59.2.173.

703 Cubrinovski, M., Ishihara, K., 2002. Maximum and minimum void
704 ratio characteristics of sands. Soils and Foundations 42, 65–78.
705 doi:10.3208/sandf.42.6_65.

706 Cucchi, V., Meredieu, C., Stokes, A., de Coligny, F., Suarez,
707 J., Gardiner, B.A., 2005. Modelling the windthrow risk
708 for simulated forest stands of Maritime pine (*Pinus pinaster*
709 Ait.). *Forest Ecology and Management* 213, 184–196. URL:
710 <http://linkinghub.elsevier.com/retrieve/pii/S0378112705002240>,
711 doi:10.1016/j.foreco.2005.03.019.

712 Dagan, G., Bresler, E., 1983. Unsaturated flow in spatially variable fields:
713 1. Derivation of models of infiltration and redistribution. *Water Resources*
714 *Research* 19, 413–420. doi:10.1029/WR019i002p00413.

715 Danjon, F., Fourcaud, T., Bert, D., 2005. Root architecture and wind-firmness
716 of mature *Pinus pinaster*. *New Phytologist* 168, 387–400. doi:10.1111/j.1469-
717 8137.2005.01497.x.

718 Danquechin Dorval, A., Meredieu, C., Danjon, F., 2016. Anchorage fail-
719 ure of young trees in sandy soils is prevented by a rigid central part of
720 the root system with various designs. *Annals of Botany* 118, 747–762.
721 doi:10.1093/aob/mcw098.

722 De Josselin De Jong, G., 1976. Rowe’s stress-dilatancy relation based on friction.
723 *Géotechnique* 26, 527–534. doi:10.1680/geot.1976.26.3.527.

724 Deirmendjian, L., Loustau, D., Augusto, L., Lafont, S., Chipeaux, C., Poirier,
725 D., Abril, G., 2018. Hydro-ecological controls on dissolved carbon dynamics in
726 groundwater and export to streams in a temperate pine forest. *Biogeosciences*
727 15, 669–691. doi:10.5194/bg-15-669-2018.

728 Dupuy, L., Fourcaud, T., Stokes, A., 2005. A Numerical Investigation into the
729 Influence of Soil Type and Root Architecture on Tree Anchorage. *Plant and*
730 *Soil* 278, 119–134. doi:10.1007/s11104-005-7577-2.

- 731 Dupuy, L.X., Fourcaud, T., Lac, P., Stokes, A., 2007. A generic 3D fi-
732 nite element model of tree anchorage integrating soil mechanics and real
733 root system architecture. *American Journal of Botany* 94, 1506–1514.
734 doi:10.3732/ajb.94.9.1506.
- 735 Ennos, A.R., 2000. The mechanics of root anchorage, in: *Advances in Botan-*
736 *ical Research*. Academic Press. volume 33, pp. 133–157. doi:10.1016/S0065-
737 2296(00)33042-7.
- 738 Fan, C.C., Su, C.F., 2009. Effect of soil moisture content on the deformation
739 behaviour of root-reinforced soils subjected to shear. *Plant and Soil* 324,
740 57–69. doi:10.1007/s11104-008-9856-1.
- 741 Fannin, R.J., Eliadorani, A., Wilkinson, J.M.T., 2005. Shear strength
742 of cohesionless soils at low stress. *Géotechnique* 55, 467–478.
743 doi:10.1680/geot.2005.55.6.467.
- 744 Fourcaud, T., Ji, J.N., Zhang, Z.Q., Stokes, A., 2007. Understanding the Impact
745 of Root Morphology on Overturning Mechanisms: A Modelling Approach.
746 *Annals of Botany* 101, 1267–1280. doi:10.1093/aob/mcm245.
- 747 Fredlund, D.G., Morgenstern, N.R., Widger, R.A., 1978. The shear
748 strength of unsaturated soils. *Canadian Geotechnical Journal* 15, 313–321.
749 doi:10.1139/t78-029.
- 750 Fredlund, D.G., Xing, A., 1994. Equations for the soil-water characteristic
751 curve. *Canadian Geotechnical Journal* 31, 521–532. doi:10.1139/t94-061.
- 752 Fukushima, S., Tatsuoka, F., 1984. Strength and deformation characteristics of
753 saturated sand at extremely low pressure. *Soils and Foundations* 24, 30–48.
- 754 Gan, J.K.M., Fredlund, D.G., Rahardjo, H., 1988. Determination of the shear

755 strength parameters of an unsaturated soil using the direct shear test. Cana-
 756 dian Geotechnical Journal 25, 500–510. doi:10.1139/t88-055.

757 Gardiner, B., Berry, P., Moulia, B., 2016. Review: Wind impacts
 758 on plant growth, mechanics and damage. Plant Science 245, 94–118.
 759 doi:10.1016/j.plantsci.2016.01.006.

760 Gardiner, B., Blennow, K., Carnus, J.M., Fleischer, P., 2010. Destruc-
 761 tive Storms in European Forests: Past and Forthcoming Impacts. Fi-
 762 nal Report to EC DG Environment. European Forest Institute. URL:
 763 <http://ec.europa.eu/environment/forests/fprotection.htm>.

764 Genet, M., Kokutse, N., Stokes, A., Fourcaud, T., Cai, X., Ji, J., Mickovski,
 765 S., 2008. Root reinforcement in plantations of *Cryptomeria japonica* D. Don:
 766 effect of tree age and stand structure on slope stability. Forest Ecology and
 767 Management 256, 1517 – 1526. doi:10.1016/j.foreco.2008.05.050.

768 Genet, M., Stokes, A., Fourcaud, T., Norris, J.E., 2010. The influence of plant
 769 diversity on slope stability in a moist evergreen deciduous forest. Ecological
 770 Engineering 36, 265 – 275. doi:10.1016/j.ecoleng.2009.05.018. special Issue:
 771 Vegetation and Slope Stability.

772 Genet, M., Stokes, A., Salin, F., Mickovski, S.B., Fourcaud, T., Du-
 773 mail, J.F., van Beek, R., 2005. The Influence of Cellulose Con-
 774 tent on Tensile Strength in Tree Roots. Plant and Soil 278, 1–9.
 775 URL: <https://doi.org/10.1007/s11104-005-8768-6>, doi:10.1007/s11104-
 776 005-8768-6.

777 Gill, M.A., 1978. A layered infiltration model for homogeneous soils. Journal of
 778 Hydrology 36, 121 – 131. doi:10.1016/0022-1694(78)90042-2.

- 779 Gonzalez-Ollauri, A., Mickovski, S.B., 2017. Plant-soil reinforcement re-
 780 sponse under different soil hydrological regimes. *Geoderma* 285, 141 – 150.
 781 doi:10.1016/j.geoderma.2016.10.002.
- 782 Govindaraju, R.S., Or, D., Kavvas, M.L., Rolston, D.E., Biggar, J., 1992.
 783 Error analyses of simplified unsaturated flow models under large uncer-
 784 tainty in hydraulic properties. *Water Resources Research* 28, 2913–2924.
 785 doi:10.1029/92WR01515.
- 786 Green, H.W., Ampt, G.A., 1911. Studies on Soil Physics. *The Journal of Agri-
 787 cultural Science* 4, 1–24. doi:10.1017/S0021859600001441.
- 788 Guan, G.S., Rahardjo, H., Choon, L.E., 2010. Shear strength equations for
 789 unsaturated soil under drying and wetting. *Journal of Geotechnical and
 790 Geoenvironmental Engineering* 136, 594–606. doi:10.1061/(ASCE)GT.1943-
 791 5606.0000261.
- 792 Hales, T.C., Miniati, C.F., 2017. Soil moisture causes dynamic adjustments to
 793 root reinforcement that reduce slope stability. *Earth Surface Processes and
 794 Landforms* 42, 803–813. doi:10.1002/esp.4039.
- 795 Houlsby, G.T., 1991. How the dilatancy of soils affects their behaviour, in:
 796 Presented at the 10th European Conference on Soil Mechanics and Foundation
 797 Engineering, University of Oxford. pp. 1–28.
- 798 Jolivet, C., Augusto, L., Trichet, P., Arrouays, D., 2007. Forest soils in the
 799 Gascony Landes Region: formation, history, properties and spatial variability.
 800 *Revue Forestière Française* LIX, 7–30. doi:10.4267/2042/8480.
- 801 Jonsson, M.J., Foetzki, A., Kalberer, M., Lundström, T., Ammann, W., Stöckli,
 802 V., 2006. Root-soil rotation stiffness of Norway spruce (*Picea abies* (L.)

803 Karst) growing on subalpine forested slopes. *Plant and Soil* 285, 267–277.
804 doi:10.1007/s11104-006-9013-7.

805 Kale, R.V., Sahoo, B., 2011. Green-Ampt Infiltration Models for Varied
806 Field Conditions: A Revisit. *Water Resources Management* 25, 3505.
807 doi:10.1007/s11269-011-9868-0.

808 Kamimura, K., Gardiner, B., Dupont, S., Guyon, D., Meredieu, C., 2016. Mech-
809 anistic and statistical approaches to predicting wind damage to individual
810 maritime pine (*Pinus pinaster*) trees in forests. *Canadian Journal of Forest*
811 *Research* 46, 88–100. doi:10.1139/cjfr-2015-0237. wOS:000370049100009.

812 Kamimura, K., Kitagawa, K., Saito, S., Mizunaga, H., 2012. Root anchor-
813 age of hinoki (*Chamaecyparis obtuse* (Sieb. Et Zucc.) Endl.) under the com-
814 bined loading of wind and rapidly supplied water on soil: analyses based on
815 tree-pulling experiments. *European Journal of Forest Research* 131, 219–227.
816 doi:10.1007/s10342-011-0508-2.

817 Kargas, G., Kerkides, P., 2011. A Contribution to the Study of the Phe-
818 nomenon of Horizontal Infiltration. *Water Resources Management* 25, 1131–
819 1141. doi:10.1007/s11269-010-9671-3.

820 Kim, J.H., Fourcaud, T., Jourdan, C., Maeght, J.L., Mao, Z., Metayer, J., Mey-
821 lan, L., Pierret, A., Rapidel, B., Roupsard, O., de Rouw, A., Sanchez, M.V.,
822 Wang, Y., Stokes, A., 2017. Vegetation as a driver of temporal variations in
823 slope stability: The impact of hydrological processes. *Geophysical Research*
824 *Letters* 44, 4897–4907. doi:10.1002/2017GL073174.

825 Konrad, J.M., Lebeau, M., 2015. Capillary-based effective stress formulation
826 for predicting shear strength of unsaturated soils. *Canadian Geotechnical*
827 *Journal* 52, 2067–2076. doi:10.1139/cgj-2014-0300.

828 Lebeau, M., Konrad, J.M., 2010. A new capillary and thin film flow model for
829 predicting the hydraulic conductivity of unsaturated porous media. *Water*
830 *Resources Research* 46. doi:10.1029/2010WR009092.

831 Lindroth, A., Lagergren, F., Grelle, A., Klemedtsson, L., Langvall, O.,
832 Weslien, P., Tuulik, J., 2009. Storms can cause Europe-wide reduc-
833 tion in forest carbon sink. *Global Change Biology* 15, 346–355. URL:
834 <https://onlinelibrary.wiley.com/doi/abs/10.1111/j.1365-2486.2008.01719.x>,
835 doi:10.1111/j.1365-2486.2008.01719.x.

836 Llano-Serna, M.A., Farias, M.M., Pedroso, D.M., Williams, D.J., Sheng, D.,
837 2018. An assessment of statistically based relationships between critical state
838 parameters. *Géotechnique* 68, 556–560. doi:10.1680/jgeot.16.T.012.

839 Lundström, T., Jonsson, M.J., Kalberer, M., 2007. The root–soil system of Nor-
840 way spruce subjected to turning moment: resistance as a function of rotation.
841 *Plant and Soil* 300, 35–49. doi:10.1007/s11104-007-9386-2.

842 Monnet, J., Boutonnier, L., 2012. Calibration of an unsaturated air–water–soil
843 model. *Archives of Civil and Mechanical Engineering* 12, 493–499.
844 doi:10.1016/j.acme.2012.07.001.

845 Moore, J.R., 2000. Differences in maximum resistive bending moments of *Pinus*
846 *radiata* trees grown on a range of soil types. *Forest Ecology and Management*
847 135, 63–71. doi:10.1016/S0378-1127(00)00298-X.

848 Neild, S.A., Wood, C.J., 1999. Estimating stem and root-anchorage flexibility
849 in trees. *Tree Physiology* 19, 141–151. doi:10.1093/treephys/19.3.141.

850 Nicoll, B.C., Gardiner, B.A., Rayner, B., Peace, A.J., 2006. Anchorage of
851 coniferous trees in relation to species, soil type, and rooting depth. *Canadian*
852 *Journal of Forest Research* 36, 1871–1883. doi:10.1139/x06-072.

853 Oberg, A., Sallfors, G., 1997. Determination of Shear Strength Parameters of
854 Unsaturated Silts and Sands Based on the Water Retention Curve. *Geotech-*
855 *nical Testing Journal* 20, 40–48. doi:10.1520/GTJ11419J.

856 Osman, N., Barakbah, S.S., 2006. Parameters to predict slope stability-
857 Soil water and root profiles. *Ecological Engineering* 28, 90–95. URL:
858 <http://www.sciencedirect.com/science/article/pii/S0925857406000784>,
859 doi:10.1016/j.ecoleng.2006.04.004.

860 Patra, C., Sivakugan, N., Das, B., Rout, S., 2010. Correlations for
861 relative density of clean sand with median grain size and compaction
862 energy. *International Journal of Geotechnical Engineering* 4, 195–203.
863 doi:10.3328/IJGE.2010.04.02.195-203.

864 Pollen, N., 2007. Temporal and spatial variability in root reinforcement of
865 streambanks: Accounting for soil shear strength and moisture. *CATENA* 69,
866 197–205. doi:10.1016/j.catena.2006.05.004.

867 Rahardjo, H., Amalia, N., Choon, L.E., Harnas, F.R., Tieng, L.T., King, F.Y.,
868 2017. Flux boundary measurements for the study of tree stability. *Landscape*
869 *and Ecological Engineering* 13, 81–92. doi:10.1007/s11355-016-0303-9.

870 Rahardjo, H., Harnas, F.R., Leong, E.C., Tan, P.Y., Fong, Y.K., Sim, E.K.,
871 2009. Tree stability in an improved soil to withstand wind loading. *Urban*
872 *Forestry & Urban Greening* 8, 237–247. doi:10.1016/j.ufug.2009.07.001.

873 Rahardjo, H., Satyanaga, A., Leong, E.C., Santoso, V.A., Ng, Y.S., 2014. Per-
874 formance of an instrumented slope covered with shrubs and deep-rooted grass.
875 *Soils and Foundations* 54, 417 – 425. doi:10.1016/j.sandf.2014.04.010.

876 Richards, L.A., 1941. A pressure-membrane extraction apparatus for soil solu-
877 tion. *Soil Science* 51, 377–386.

- 878 Rouse, P.C., 2018. Relation between the critical state friction angle of sands
879 and low vertical stresses in the direct shear test. *Soils and Foundations* 58,
880 1282 – 1287. doi:10.1016/j.sandf.2018.06.005.
- 881 Rowe, P.W., Taylor, G.I., 1962. The stress-dilatancy relation for static equilib-
882 rium of an assembly of particles in contact. *Proceedings of the Royal Soci-*
883 *ety of London. Series A. Mathematical and Physical Sciences* 269, 500–527.
884 doi:10.1098/rspa.1962.0193.
- 885 Sadrekarimi, A., Olson, S.M., 2011. Critical state friction angle of sands.
886 *Géotechnique* 61, 771–783. doi:10.1680/geot.9.P.090.
- 887 Sagi, P., Newson, T., Miller, C., Mitchell, S., 2019. Stem and root sys-
888 tem response of a Norway spruce tree (*Picea abies* L.) under static load-
889 ing. *Forestry: An International Journal of Forest Research* 92, 460–472.
890 URL: <https://academic.oup.com/forestry/article/92/4/460/5524738>,
891 doi:10.1093/forestry/cpz042.
- 892 Sammut C., W.G.I., 2010. Leave-One-Out Cross-Validation, in: Sammut, C.,
893 Webb, G.I. (Eds.), *Encyclopedia of Machine Learning*. Springer US, Boston,
894 MA, pp. 600–601. doi:10.1007/978-0-387-30164-8_469.
- 895 Schelhaas, M.J., 2008. The wind stability of different silvicultural systems for
896 Douglas-fir in the Netherlands: a model-based approach. *Forestry: An Inter-*
897 *national Journal of Forest Research* 81, 399–414. doi:10.1093/forestry/cpn028.
- 898 Schwarz, M., Cohen, D., Or, D., 2010. Root-soil mechanical interactions during
899 pullout and failure of root bundles. *Journal of Geophysical Research: Earth*
900 *Surface* 115, 1–19. doi:10.1029/2009JF001603.
- 901 Seidl, R., Schelhaas, M.J., Rammer, W., Verkerk, P.J., 2014. Increasing forest

disturbances in Europe and their impact on carbon storage. *Nature Climate Change* 4, 806–810. doi:10.1038/nclimate2318.

Shanker, K., Basudhar, P.K., Patra, N.R., 2006. Uplift capacity of pile groups embedded in sands: predictions and performance. *Soils and Foundations* 46, 605–612. doi:10.3208/sandf.46.605.

Shelke, A., Patra, N.R., 2008. Effect of Arching on Uplift Capacity of Pile Groups in Sand. *International Journal of Geomechanics* 8, 347–354. doi:10.1061/(ASCE)1532-3641(2008)8:6(347).

Simon, A., Collison, A.J.C., 2002. Quantifying the mechanical and hydrologic effects of riparian vegetation on streambank stability. *Earth Surface Processes and Landforms* 27, 527–546. doi:10.1002/esp.325.

Stocker, T.F., Qin, D., Plattner, G.K., Tignor, M.M.B., Allen, S.K., Boschung, J., Nauels, A., Xia, Y., Bex, V., Midgley, P.M. (Eds.), 2014. *Climate Change 2013: The Physical Science Basis*. Cambridge Univ Press, Cambridge, United Kingdom and New York, NY, USA. doi:10.1017/CBO9781107415324.

Stokes, A., Norris, J.E., van Beek, L.P.H., Bogaard, T., Cammeraat, E., Mickovski, S.B., Jenner, A., Di Iorio, A., Fourcaud, T., 2008. How Vegetation Reinforces Soil on Slopes, in: Norris, J.E., Stokes, A., Mickovski, S.B., Cammeraat, E., van Beek, R., Nicoll, B.C., Achim, A. (Eds.), *Slope Stability and Erosion Control: Ecotechnological Solutions*. Springer Netherlands, Dordrecht, pp. 65–118. doi:10.1007/978-1-4020-6676-4_4.

Tatsuoka, F., Sakamoto, M., Kawamura, T., Fukushima, S., 1986. Strength and deformation characteristics of sand in plane strain compression at extremely low pressure. *Soils and Foundations* 26, 65–84. doi:10.3208/sandf1972.26.65.

Vanitha, L., Patra, N.R., Chandra, S., 2007. Uplift capacity of pile

927 group anchors. *Geotechnical and Geological Engineering* 25, 339–347.
928 doi:10.1007/s10706-006-9114-3.

929 Veylon, G., Ghestem, M., Stokes, A., Bernard, A., 2015. Quantification of me-
930 chanical and hydric components of soil reinforcement by plant roots. *Canadian*
931 *Geotechnical Journal* 52, 1839–1849. doi:10.1139/cgj-2014-0090.

932 Wen, B.P., Yan, Y.J., 2014. Influence of structure on shear characteristics of
933 the unsaturated loess in lanzhou, china. *Engineering Geology* 168, 46–58.
934 doi:10.1016/j.enggeo.2013.10.023.

935 Whisler, F.D., Bouwer, H., 1970. Comparison of methods for calculating ver-
936 tical drainage and infiltration for soils. *Journal of Hydrology* 10, 1 – 19.
937 doi:10.1016/0022-1694(70)90051-X.

938 Wu, T.H., 2013. Root reinforcement of soil: review of analytical models, test
939 results, and applications to design. *Canadian Geotechnical Journal* 50, 259–
940 274. doi:10.1139/cgj-2012-0160.

941 Yang, K.H., Uzuoka, R., Thuo, J.N., Lin, G.L., Nakai, Y., 2017. Coupled hydro-
942 mechanical analysis of two unstable unsaturated slopes subject to rainfall in-
943 filtration. *Engineering Geology* 216, 13–30. doi:10.1016/j.enggeo.2016.11.006.

944 Yang, M., Défossez, P., Danjon, F., Fourcaud, T., 2014. Tree stability under
945 wind: simulating uprooting with root breakage using a finite element method.
946 *Annals of Botany* 114, 695–709. doi:10.1093/aob/mcu122.

947 Yang, M., Défossez, P., Danjon, F., Fourcaud, T., 2018. Analyzing key factors
948 of roots and soil contributing to tree anchorage of *Pinus* species. *Trees* 32,
949 703–712. doi:10.1007/s00468-018-1665-4.

950 Zapata, C.E., Houston, W.N., Houston, S., Walsh, K.D., 2000. Soil-
951 water characteristic curve variability, in: *Proceedings of Sessions of Geo-*

952 Denver 2000 - Advances in Unsaturated Geotechnics, GSP 99, pp. 84-124.
953 doi:10.1061/40510(287)7. sessions of Geo-Denver 2000 - Advances in Unsat-
954 urated Geotechnics, GSP 99 ; Conference date: 05-08-2000 Through 08-08-
955 2000.

Trees	H	DBH	V_{root}	SRL	S_W	S_{CW}	S_T
11	10.12	0.1623	32786	0.70	1233.3	1151.3	1986.0
12	10.00	0.1814	41793	0.57	761.8	1537.8	1833.7
13	11.48	0.1751	40592	0.58	1807	3351.3	1375.2
31	9.70	0.1687	33234	0.78	1013.8	2049.8	1885.6
32	9.38	0.1687	25513	0.79	849.1	1372.4	1918.1
33	9.78	0.1783	35984	0.57	1780.6	875.0	1467.6
14	10.62	0.1798	34027	0.59	1412.7	1184.3	2158.7
15	10.40	0.1846	33336	0.52	1317.4	797.7	2853.5
16	11.15	0.1783	39816	0.57	1357.3	1446.2	2019.6
34	10.07	0.191	34673	0.58	140.9	1592.6	2196.3
35	11.65	0.1783	31520	0.53	319	2056.2	2140.2
36	10.65	0.1655	21775	1.15	2323	704.6	1607.4
Model	10.41	0.176	-	0.66	1193	1509.9	1953.5

H = Tree height (m), DBH = Stem diameter diameter at 1.3 m (m)
 V_{root} = Root system volume, stump included (cm^3)
 SRL = Specific Root Length, stump excluded ($cm.cm^{-3}$)
 S_W = root surface in the winching direction (cm^2)
 S_{CW} = root surface in the counter winching direction (cm^2)
 S_T = tap root surface (cm^2)

Table 1: Root architectural data of the 12 tree root systems after excavation and 3D digitizing and mean values used for simulations.

Test	11	12	13	31	32	33	14	15	16	34	35	36
k_r	3.52	3.63	3.70	3.10	2.25	3.91	3.36	3.01	3.11	3.61	3.56	1.69
M_c	14.33	14.73	16.10	12.78	10.61	14.10	15.07	13.94	14.88	12.12	13.68	7.92
α_r^c	8.1	10.0	13.8	13.7	12.9	13.2	13.7	15.4	10.5	8.0	8.8	18.0
Soil dry bulk density ρ_d (Mgm^{-3})												
0-10 cm	1.234	1.232	1.22	1.376	1.085	1.188	1.101	1.301	1.339	1.176	1.217	1.359
10-40 cm	1.596	1.52	1.348	1.333	1.373	1.281	1.49	1.225	1.616	1.453	1.42	1.256
40-60 cm	1.632	1.552	1.578	1.633	1.582	1.517						
Soil gravimetric water content w_n (-)												
0-10 cm	0.154	0.153	0.138	0.148	0.178	0.165	0.264	0.183	0.222	0.185	0.269	0.192
10-40 cm	0.063	0.072	0.112	0.132	0.135	0.107	0.213	0.267	0.206	0.245	0.288	0.307
40-60 cm	0.1	0.085	0.068	0.108	0.1	0.07	Sat	Sat	Sat	Sat	Sat	Sat
Saturation ratio S_r (-)												
0-10 cm	0.139	0.138	0.122	0.166	0.127	0.139	0.194	0.183	0.236	0.153	0.237	0.210
10-40 cm	0.100	0.101	0.121	0.139	0.151	0.104	0.286	0.238	0.338	0.310	0.347	0.287
40-60 cm	0.169	0.126	0.105	0.182	0.155	0.098	Sat	Sat	Sat	Sat	Sat	Sat

k_r = initial angular stiffness of the root system ($kN.m/^\circ$),
 M_c = critical overturning moment ($MN.m$), α_r^c = critical angle ($^\circ$)
 w_n and ρ_d -values correspond to the average of four measurements

Table 2: Field data for the pulling tests under wet soil conditions in 2012 and very wet conditions in 2013.

M_c	
0.33	H
0.349	DBH
0.878****	V_{root}
-0.847****	SRL
-0.117	S_W
0.430	S_{CW}
0.070	S_T
0.002	ρ_d (0-10 cm)
-0.443	ρ_d (10-40 cm)
-0.247	ρ_d (40-60 cm)
-0.168	w_n (0-10 cm)
0.421	w_n (10-40 cm)
-0.101	w_n (40-60 cm)

Table 3: Correlation analysis for the critical turning moment with root architectural data and soil conditions.

Sample	e	w_n	S_r	σ_n	τ_f
Layer 10-40 cm					
L2-020-6	00.73	0.206	0.430	6.01	4.50
L2-020-8	0.71	0.199	0.416	8.05	7.46
L2-020-13	0.79	0.196	0.409	13.56	8.88
L2-015-3	0.84	0.167	0.349	3.17	3.08
L2-015-6	0.84	0.161	0.337	6.01	4.27
L2-015-8	0.84	0.167	0.348	8.05	5.57
L2-015-13	0.84	0.164	0.342	13.57	8.10
L2-010-3	0.84	0.109	0.228	3.17	3.00
L2-010-6	0.84	0.1	0.209	6.01	5.09
L2-010-8	0.84	0.106	0.221	8.05	5.21
L2-010-13	0.84	0.109	0.228	13.57	9.00
L2-sat-3	0.84	0.24	0.501	3.17	2.50
Layer 40-60 cm					
L3-020-3	0.65	0.188	0.755	3.17	4.52
L3-020-6	0.65	0.19	0.767	6.01	7.70
L3-020-8	0.65	0.211	0.848	8.05	8.04
L3-020-13	0.65	0.197	0.794	13.56	8.60
L3-015-3	0.65	0.127	0.512	3.17	5.45
L3-015-6	0.65	0.15	0.603	6.01	8.53
L3-015-8	0.65	0.181	0.73	8.04	9.30
L3-015-13	0.65	0.144	0.58	13.57	12.43
L3-010-3	0.65	0.094	0.38	3.17	4.50
L3-010-6	0.65	0.103	0.416	6.01	7.11
L3-010-8	0.65	0.101	0.405	8.05	7.70
L3-sat-3	0.69	0.258	0.973	3.17	4.80
L3-sat-6	0.69	0.263	0.993	6.01	4.80
L3-sat-8	0.69	0.256	0.965	8.05	6.80
L3-sat-13	0.69	0.259	0.979	13.57	9.60

e = void ratio (-), w_n = gravimetric water content (-),
 σ_n = vertical stress (kPa), τ_f

Table 4: The soil shear strength τ_f measured with the direct shear tests on the soil samples of layers 10-40 cm and 40-60cm corresponding to two void ratios e for different saturation ratio S_r and vertical stress σ_n . Each sample is designed by the layer (L2 or L3), the initial water content w_n from 0.10 to saturation and the vertical stress applied during tests from 3.17 to 13.57 kPa

	M_0	l_W^φ	l_{CW}^φ	l_T^φ	l_W^ψ	l_{WC}^ψ	l_T^ψ	R^2
Regression on all tests								
	8.40	3.28	-0.32	1.12	3.87	9.69	7.12	0.91
Regressions on tests by leaving one test out								
Mean	8.48	3.28	-0.23	1.10	3.67	9.01	6.99	0.89
S. Dev.	0.93	0.51	0.38	0.24	0.98	2.30	1.00	0.04
$M_0 = \text{constant factor (kN.m)}$								
$l_i^j = \text{the lever arm coefficients (m)}$								

Table 5: Parameters values obtained by multi-linear regression of the field critical turning moment data.

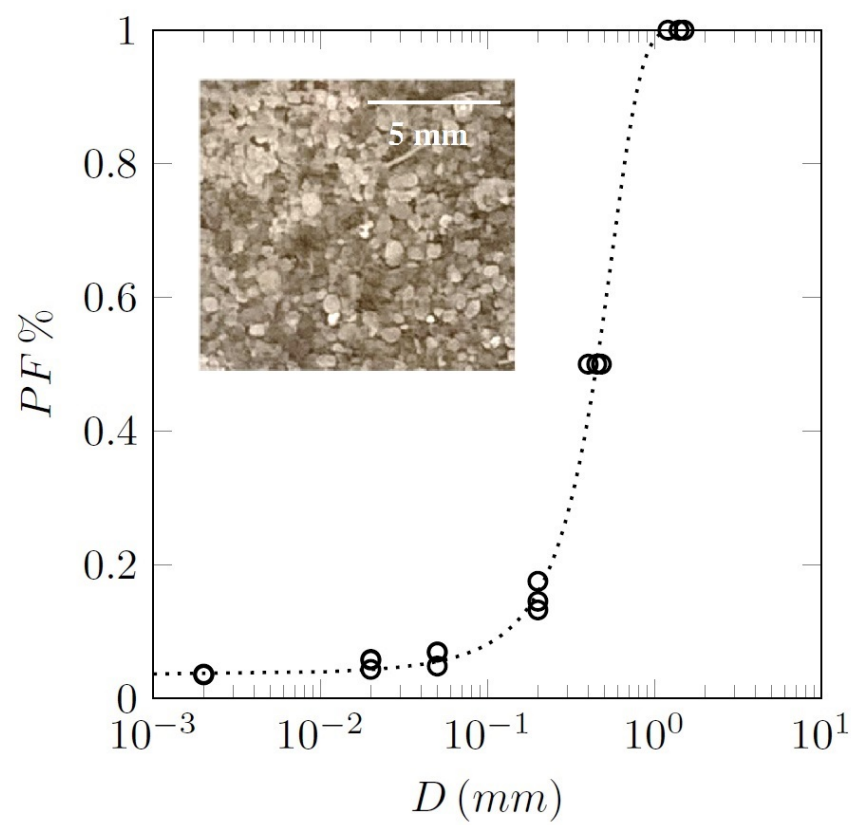


Figure 1: Particle size distribution of the substrate.



Figure 2: Root system after winching test. The zoom focus on the roots in the counterwinch sector that were pulled out the soil.

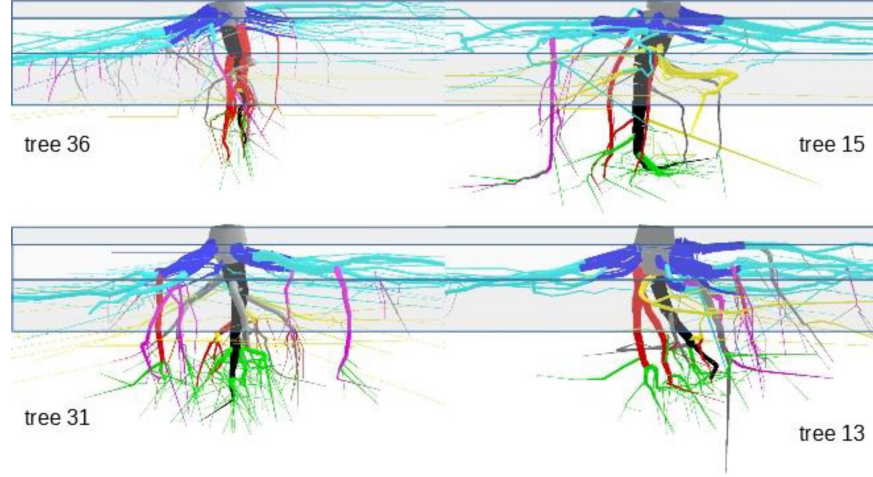


Figure 3: 3D reconstruction of four tree root systems. Segments were coloured according to their compartments according to Danquechin Dorval et al. (2016): (1) stump in grey, (2) taproot in black, (3) zone of rapid taper (ZRT) of horizontal shallow roots in dark blue, (4) horizontal shallow roots beyond the ZRT in light blue, (5) sinker roots branching from the ZRT in red, (6) sinker roots beyond the ZRT in magenta, (7) intermediate-depth horizontal roots in yellow, (8) deep roots in green, (9) oblique roots in dark grey. The 0-10, 10-30 and 30-60 depth soil layers are represented in shades of grey. The width of the whole figure is 5 m, with trees winched to the right. A reconstruction of root systems 34 and 35, perpendicular to the winching direction, can be found in Danquechin Dorval et al. (2016).

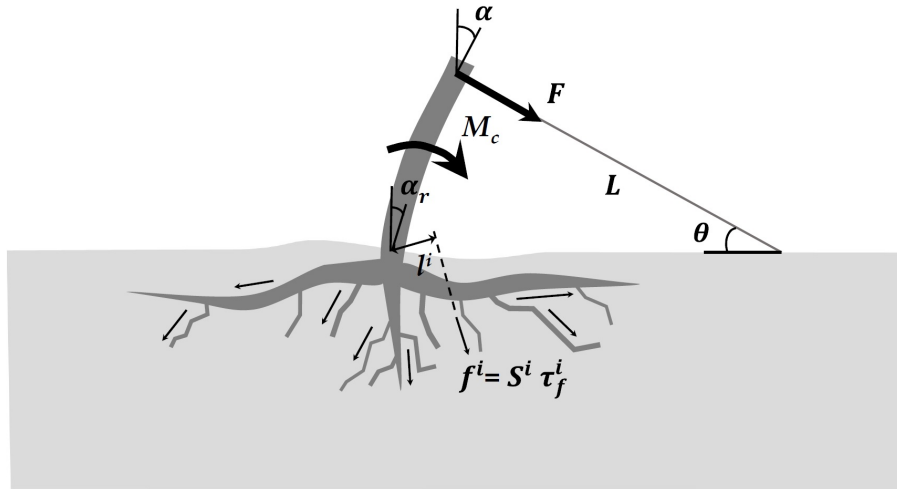


Figure 4: Mechanical model of the overturning root system. Each root i contributed to the critical resisting moment by its pullout resistance f^i and lever arm l^i .

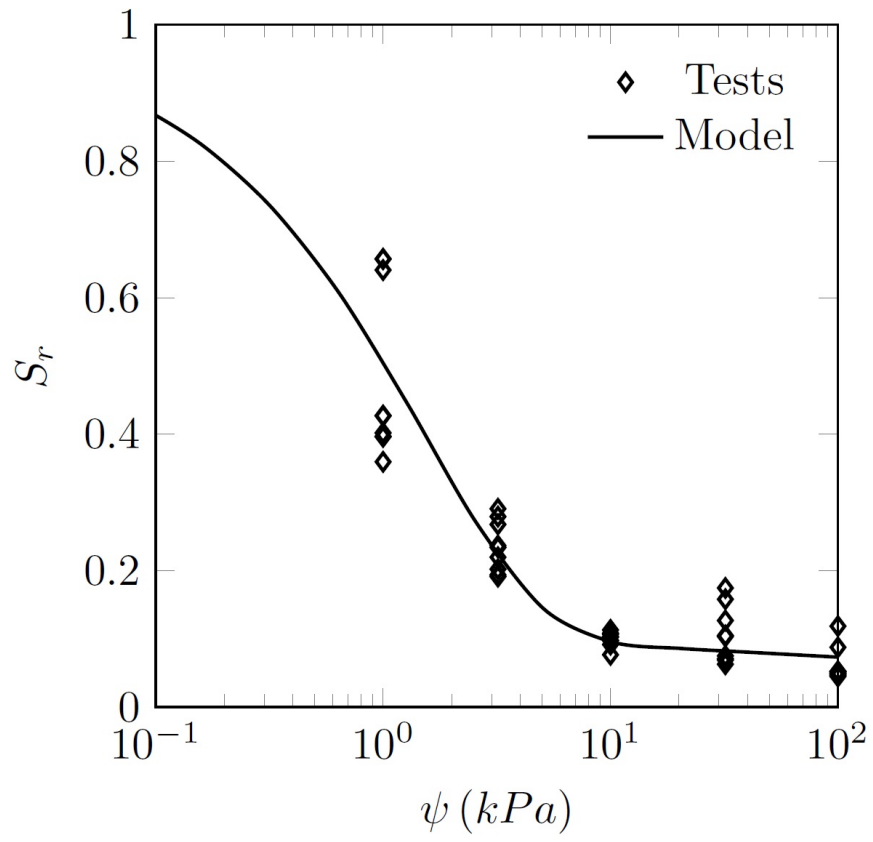


Figure 5: The water retention curve calibrated from the pressure plate tests for matric suction between 1 and 100 kPa.

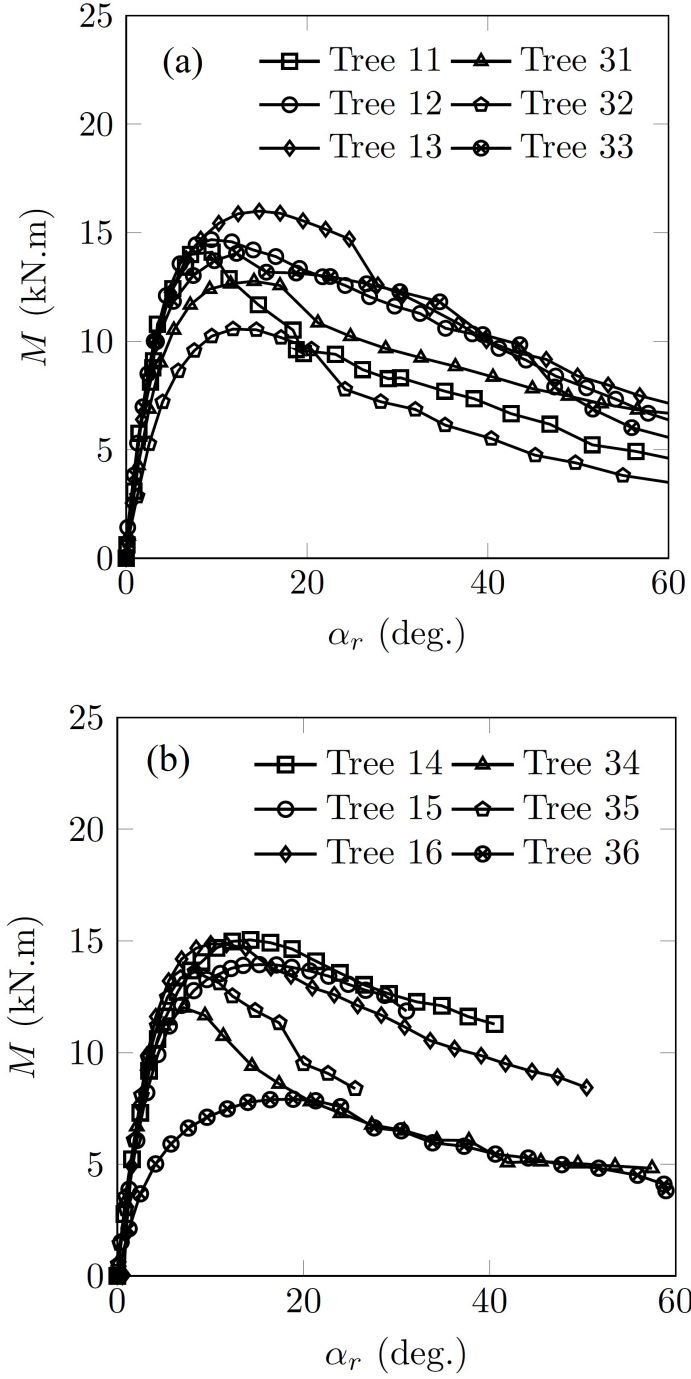


Figure 6: Response curves of turning moment measured for the 12 trees, 6 in 2012 (a) and 6 in 2013 (b) as function of the deflection angle at base of the tree α_r . The curves characterize a typical response of elasto-plastic material with a linear elastic part at small angle and a transition to plastic and damage part at higher angle. The maximum value of turning moment is considered as the ultimate rupture of the soil-root system and defines the critical bending moment M_c .

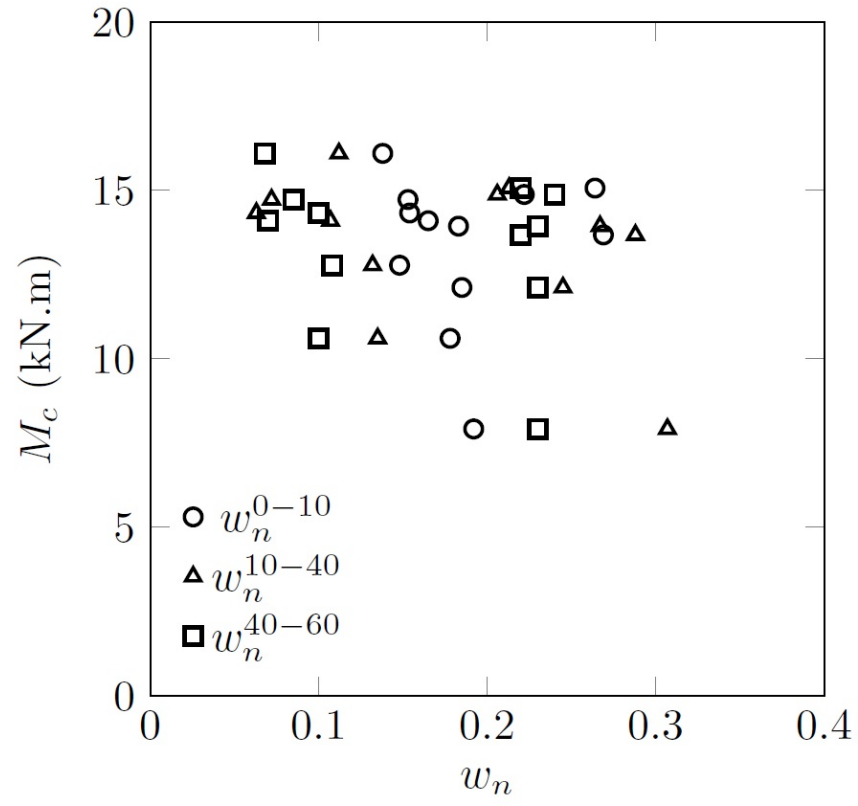


Figure 7: The critical turning moment M_c as a function of soil water contents representative of the three soil layers 0-10 cm, 10-40 cm and 40-60 cm.

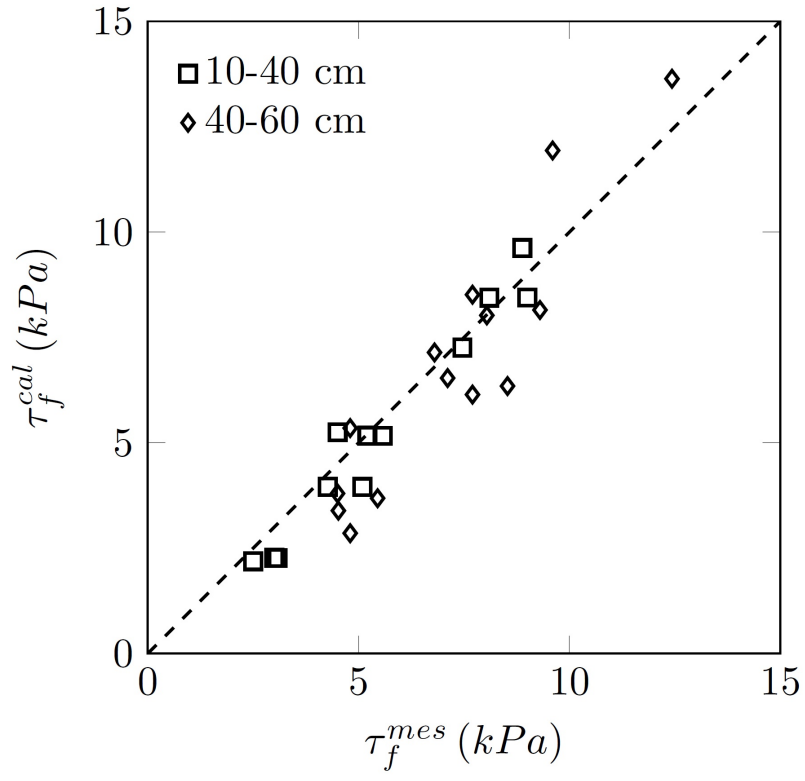


Figure 8: Comparison of the shear strength measured by direct shear tests (τ_{mes}) to the one calculated by the model (τ_{cal}). The determination coefficient is $R^2 = 0.80$.)

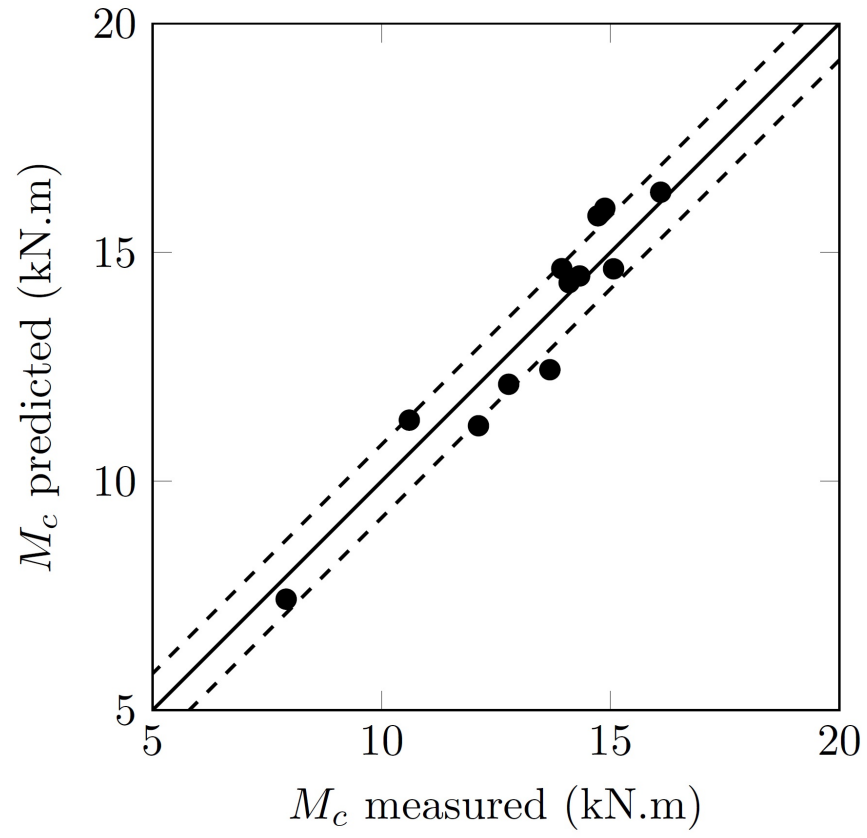


Figure 9: Representation of the critical turning moments measured during winching tests and predicted by the model ($R^2=0.90$). The dashed lines represent the regression line \pm the standard error.

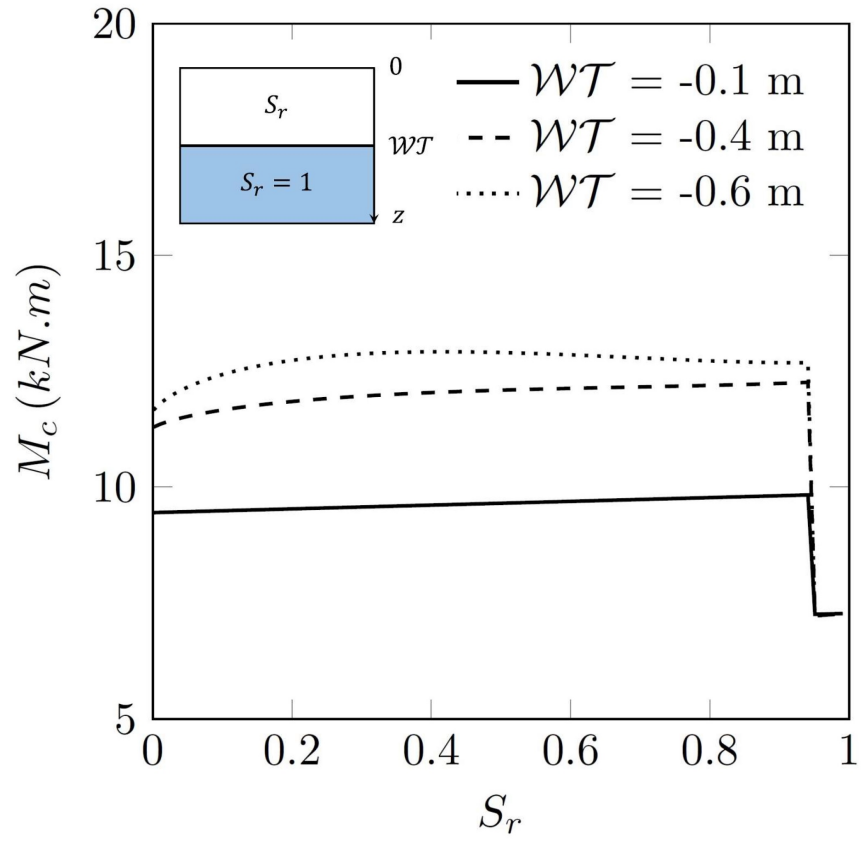


Figure 10: Representation of the critical turning moments predicted by the model as a function of water table level (\mathcal{WT}) and soil saturation ratio above the water table level.

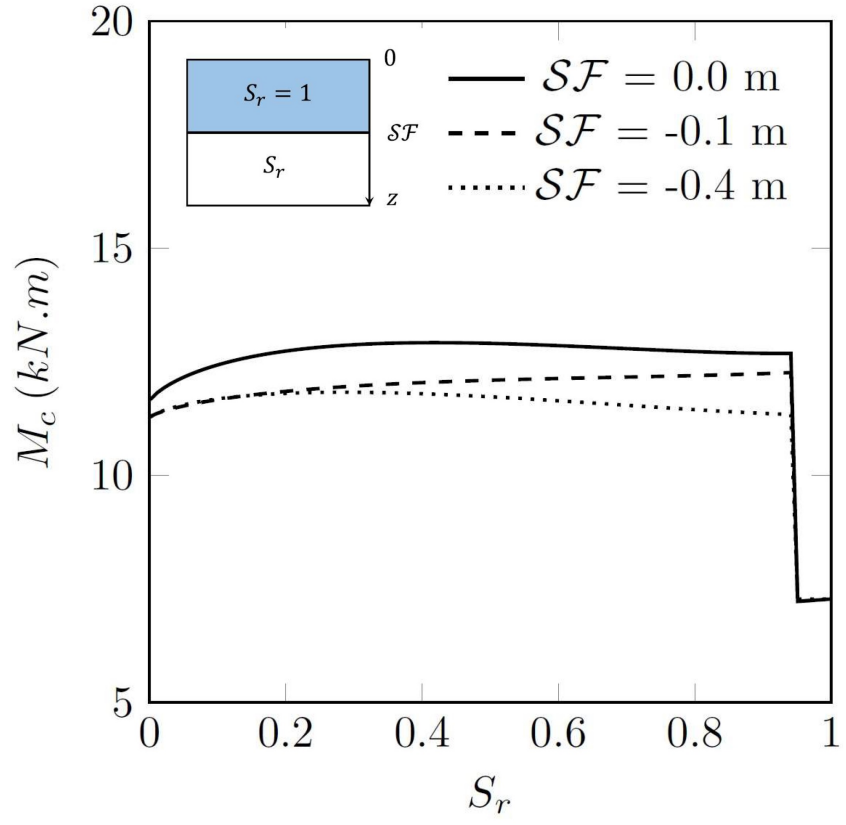


Figure 11: Simulation of the critical turning moment as a function of saturation front level (\mathcal{SF}) and soil saturation ratio below the saturation front.

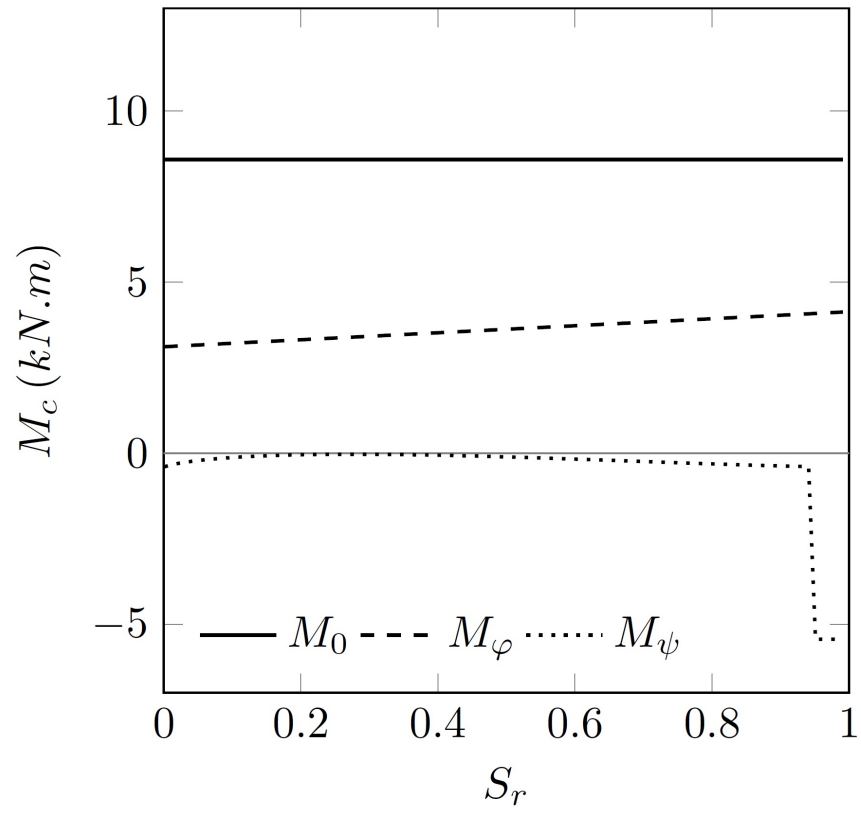


Figure 12: Representation of the components of the resisting moment for a water table level $\mathcal{WT} = -0.40$ m.